

Influence of Two Different Salt Mixture Combinations of Na_2SO_4 - NaCl - NaVO_3 on Hot Corrosion Behavior of Ni-Base Superalloy Nimonic263 at 800 °C

Venkateswararao Mannava, A. SambasivaRao, M. Kamaraj, and Ravi Sankar Kottada

(Submitted August 4, 2018; in revised form December 4, 2018; published online January 22, 2019)

Isothermal hot corrosion behavior of Nimonic263 alloy was studied under the influence of two different salt mixtures of 87.5 wt.% Na_2SO_4 + 5 wt.% NaCl + 7.5 wt.% NaVO_3 (3SM) and 74 wt.% Na_2SO_4 + 21.7 wt.% NaCl + 4.3 wt.% NaVO_3 (3SM-A) and also without salt mixtures up to 500 h at 800 °C. Corrosion kinetics showed that 3SM-A is more aggressive than 3SM. Multiple oxides, spinels, sulfides, vanadate compounds, and volatile compounds were observed during various hot corrosion reactions. The volatile compounds NaClO_3 and CrMoO_3 , and SO_3 gas are attributed to the weight loss under both 3SMs. The Na_2SO_4 of 3SM prevailed till 400 h, but that of 3SM-A disappeared within 5 h, as established conclusively by Raman spectra analysis. The sulfides plus internal oxide zone increased with the increased exposure duration as evident from the extensive EPMA analysis. Based on the critical analysis of corrosion kinetics and detailed microstructural characterization, fluxing and sulfidation followed by oxidation are identified as plausible hot corrosion mechanisms under both 3SMs. Besides, chlorination and high-temperature oxidation mechanisms occur under 3SM-A condition.

Keywords EPMA, hot corrosion, Ni-base superalloys, oxidation, Raman spectroscopy, XRD

1. Introduction

The Ni-base superalloys have been used as rotor blades, disks, nozzle guide vanes, combustion chamber casings, and liners in aircraft and marine turbine engines due to their excellent high-temperature creep resistance and outstanding oxidation resistance (Ref 1). Nevertheless, turbine engine components made of these alloys are vulnerable to molten salts such as Na_2SO_4 , NaCl , V_2O_5 , and NaVO_3 and prone to damage the protective oxide scales. The primary reason for the formation of molten salts is due to the infiltrated air and residual fuels in aircraft and marine gas turbine engines. Sulfur (S), vanadium (V), and lead (Pb) from fuel, and sodium (Na) which is present in the air remain as impurities even after combustion (Ref 2).

These impurities react with surrounding oxygen and form SO_2 and V_2O_5 oxides, and these oxides react again with Na_2O to form Na_2SO_4 and NaVO_3 , respectively. In the marine environment, sea water is the significant source for NaCl . So,

NaCl reacts with sulfur dioxide and oxygen, and form Na_2SO_4 . Thus, Na_2SO_4 is a major contaminant in the marine environment, whereas V_2O_5 is a primary major contaminant in an aircraft environment (Ref 2).

Hot corrosion is defined as accelerated oxidation resulting from the salt contaminants such as Na_2SO_4 , NaCl , and V_2O_5 that combine to form molten deposits on the external surface of components (Ref 3). Based on the alloy composition, gas composition, temperature, and surface morphology, hot corrosion is broadly classified into two types: high-temperature hot corrosion (HTHC) or Type I hot corrosion that occurs in the temperature range of 800-950 °C and low-temperature hot corrosion (LTHC) or Type II hot corrosion that happens in the temperature range of 600-750 °C. In HTHC, Na_2SO_4 is in the molten state, whereas during LTHC, Na_2SO_4 - MSO_4 (M=Ni, Co, and Fe) forms eutectics, and hence, it is in the molten state.

In the late 1960 s, hot corrosion was recognized as a dangerous problem both in aircraft and marine gas turbine engines, and Na_2SO_4 was perceived to be the only salt that damages the engine components at > 800 °C. Subsequently, extensive research was carried out with the deposition of Na_2SO_4 at different gas mixture ratios of SO_2/O_2 and shown that hot corrosion is a cyclic process, i.e., sulfidation followed by oxidation (Ref 4). Successively, Bornstein and DeCrescente (Ref 5, 6) demonstrated that hot corrosion follows the fluxing model/mechanism (either basic or acidic fluxing), where the reaction occurs between molten salts and oxides on the surface of the alloys. In basic fluxing, oxides react with O^{2-} or Na_2O when SO_3 partial pressure is less, whereas oxides dissociate into corresponding cations and O^{2-} ions in acidic fluxing. Subsequent studies of Goebel et al. (Ref 7, 8) on hot corrosion behavior of different alloys with Na_2SO_4 deposition corroborated the occurrence of the fluxing mechanism. After that, V_2O_5 presence along with Na_2SO_4 is known to play a crucial role in an aircraft environment, and consequently, a lot of research was performed and concluded that the formation of NaVO_3 by the

Electronic supplementary material The online version of this article (<https://doi.org/10.1007/s11665-019-3866-4>) contains supplementary material, which is available to authorized users.

Venkateswararao Mannava, M. Kamaraj, and Ravi Sankar Kottada, Department of Metallurgical and Materials Engineering, Indian Institute of Technology Madras, Chennai 600036, India; A. SambasivaRao, Structural Failure Analysis Group, Defence Metallurgical Research Laboratory, Hyderabad 500058, India. Contact e-mail: venki.2484@gmail.com.

combination of Na₂SO₄ and V₂O₅ enhances the oxidation behavior (Ref 9-12).

On the other hand, Johnson et al. (Ref 13) anticipated that NaCl is the primary corrodent in the marine environment, and reported that NaCl destroys the oxide layers and accelerates the oxidation. Further, Wortman et al. (Ref 14) observed that NaCl completely reacts with SO₂ and forms Na₂SO₄, and described that Na₂SO₄ accelerates the oxidation behavior. Subsequently, Luthra (Ref 15, 16) worked on the Co-base alloys and reported that Na₂SO₄ deposition together with sufficient SO₃ forms Na₂SO₄-CoSO₄ eutectics in the marine environment, which accelerates the oxidation behavior below 800 °C. Successively, Kameswari (Ref 17) observed that as long as the gas turbine engine runs in a marine environment, some fraction of NaCl deposition will be present along with Na₂SO₄ and reported that NaCl aids Na₂SO₄ to enhance the oxidation behavior. Later, Nicholls and Stephenson (Ref 18) studied the hot corrosion behavior of IN738 superalloy with NaCl deposition in the presence of O₂-SO₂-SO₃ gas mixtures at 700 °C and described that NaCl destroys the protective oxide scales and accelerates the oxidation behavior.

In succession, substantial work has been reported on hot corrosion (either electrochemical or weight measurement studies) in a marine environment with Na₂SO₄/NaCl and different mixture ratios of Na₂SO₄ and NaCl. The relevant information from these hot corrosion studies is presented in Table 1. A close inspection of

Table 1 suggests that (a) among various weight ratios of Na₂SO₄-NaCl salt mixtures, more than 15 wt.% addition of NaCl is more aggressive in the temperature range of 650-900 °C, and (b) there are no hot corrosion studies with the addition of V₂O₅ or NaVO₃ to Na₂SO₄-NaCl salt mixtures to mimic the marine environment. Recently, hot corrosion studies were conducted on IN718 and IN738LC superalloys with different three salt mixture depositions of Na₂SO₄, NaCl, V₂O₅/NaVO₃ at different temperatures and demonstrated that three salt mixtures significantly accelerate the oxidation behavior (Ref 28-32).

A detailed literature survey and critical analysis of Mannava et al. (Ref 29) brought out the differences in impurities in different fuels, which are used in aircraft and marine gas turbine engines. Among them, the majority of the residual fuel in gas turbine engines contains a significant amount of vanadium as an impurity, which converts as V₂O₅ (Ref 33). Since vanadium is an unavoidable impurity that originates from the residual fuel, hot corrosion study to mimic the marine environment should have the salt mixture combination of Na₂SO₄, NaCl and V₂O₅/NaVO₃.

Nimonic263 is one of the promising wrought Ni-base superalloys and is used in various gas turbine engine components such as stators and combustion chamber liners (Ref 34). Based on the detailed literature survey and discussion presented above on hot corrosion studies on superalloys, it is evident that there are hardly any extensive and detailed studies

Table 1 Previous reports on hot corrosion behavior of Ni- and Co-base alloys at different temperatures carried out using salt mixtures of Na₂SO₄ and NaCl

Author/year	Alloy	Temperature °C	Salt mixture (in wt.%)	Remark
Sequeira et al. (Ref 19)	Nimonic105	900	Na ₂ SO ₄ , NaCl 99Na ₂ SO ₄ -1NaCl 90Na ₂ SO ₄ -10 NaCl 85Na ₂ SO ₄ -15 NaCl 75Na ₂ SO ₄ -25 NaCl 65Na ₂ SO ₄ -35 NaCl 50Na ₂ SO ₄ -50 NaCl 30Na ₂ SO ₄ -70 NaCl	Not much effect on hot corrosion with the addition of NaCl (up to 15%) to Na ₂ SO ₄ . Around 15-35% NaCl is more aggressive. Cl ⁻ melts required some incubation period to accelerate the sulfidation.
Siva Kumar et al. (Ref 20)	Ni-Cr and Ni-Cr-Al Ni-Cr-Ti	750-900	85Na ₂ SO ₄ -15 NaCl	Ni-Cr and Ni-Cr-Ti alloys undergo uniform attack, whereas Ni-Cr-Al alloy undergoes blistering corrosion.
Gurrappa (Ref 21)	CM247LC	900	95Na ₂ SO ₄ -5NaCl 90Na ₂ SO ₄ -10NaCl 85Na ₂ SO ₄ -15NaCl 80Na ₂ SO ₄ -20NaCl	Corrosion rate is higher with 20 wt.% of NaCl than 10 wt.%.
Zeng et al. (Ref 22)	B1900	800	75Na ₂ SO ₄ -25 NaCl	Na ₂ SO ₄ -Na ₂ MoO ₄ -MoO ₃ mixture formation enhances corrosion rate.
Meiheng Li et al. (Ref 23)	SC Ni-base superalloy	900	75Na ₂ SO ₄ -25 NaCl	Accelerated oxidation occurs due to the formation of volatile chlorides.
Liu et al. (Ref 24)	M38G	800-950	75Na ₂ SO ₄ -25 NaCl	Salt mixture damages the oxide layer and enhances the corrosion rate. Pre-oxidation treatment improves the hot corrosion resistance.
Sidhu et al. (Ref 25)	Super 75	800	75Na ₂ SO ₄ -25 NaCl	NaCl reacts with oxides and forms volatile chlorides. These chlorides diffuse out along the grain boundaries and form pits.
Zhang et al. (Ref 26)	K40S	900	75Na ₂ SO ₄ -25 NaCl	Cl ⁻ ions accelerate the oxides through fluxing mechanisms.
Lei Zheng et al. (Ref 27)	Rene 95	650- 750	75Na ₂ SO ₄ -25 NaCl	As time increases, weight loss increases and oxidation followed by sulfidation mechanism occurs.

on hot corrosion behavior of Nimonic263 either with $\text{Na}_2\text{SO}_4/\text{NaCl}$ or with salt mixtures of $\text{Na}_2\text{SO}_4\text{-NaCl}$. Moreover, there are no hot corrosion studies with the addition of $\text{V}_2\text{O}_5/\text{NaVO}_3$ to $\text{Na}_2\text{SO}_4\text{-NaCl}$ salt mixtures on this alloy.

Therefore, to fill this gap, the present study focuses on isothermal hot corrosion behavior of Nimonic263 at 800 °C with two different salt mixture combinations having $\text{NaVO}_3/\text{V}_2\text{O}_5$ addition to $\text{Na}_2\text{SO}_4 + \text{NaCl}$ combination: (a) 87.5 wt.% $\text{Na}_2\text{SO}_4 + 5$ wt.% $\text{NaCl} + 7.5$ wt.% NaVO_3 (3SM) and (b) 74 wt.% $\text{Na}_2\text{SO}_4 + 21.7$ wt.% $\text{NaCl} + 4.3$ wt.% NaVO_3 (3SM-A). To elucidate the plausible hot corrosion mechanism of Nimonic263 with three salt mixtures at 800 °C, comprehensive microstructural characterization and analysis were carried out using XRD, Raman spectroscopy, SEM/EDS, and EPMA. Further, the difference in hot corrosion behavior with 3SM and 3SM-A salt mixtures was also explained.

2. Experimental Materials and Methods

The wrought Nimonic263 superalloy was used in the present study. The chemical composition (wt.%) of Nimonic263 as measured by Optical Emission Spectroscopy (OES) is Cr-20, Co-21, Al-0.45, Ti-2.3, Mo-5.5, Fe-0.7, Mn-0.6, C-0.03, and Ni-balance. Prior to heat treatment, the hot corrosion specimens with dimensions of 15 mm diameter and 2 mm thickness were prepared from a rod of 15 mm diameter and 1 m length and then vacuum-sealed in a fused silica quartz tube. Subsequently, specimens were subjected to standard two-stage heat treatment: annealing at 1150 °C for 2 h and water quenching and followed by annealing at 800 °C for 8 h, and air cooling. Successively, samples were ground with SiC grit papers 220-1000 and then cleaned ultrasonically with acetone for 15 min and dried. Prior to spraying the saturated solution of 87.5 wt.% $\text{Na}_2\text{SO}_4 + 5$ wt.% $\text{NaCl} + 7.5$ wt.% NaVO_3 (3SM) and 74 wt.% $\text{Na}_2\text{SO}_4 + 21.7$ wt.% $\text{NaCl} + 4.3$ wt.% NaVO_3 (3SM-A), the sample weight was measured by using weighing balance (accuracy of 0.1 mg). Subsequently, the samples were fixed in rotating holder which is connected to the oven. The oven temperature was set at 135 °C.

The saturated solutions of 3SM and 3SM-A were prepared and sprayed on the rotating samples by using a spray gun from the distance of 45 cm from the sample holder with the air pressure of 2.5 bar via a compressor. Then, 3SMs were deposited on the samples and measured the weight of the samples at regular intervals by taking out the samples repeatedly from the oven until $\sim 2.5 \pm 0.2$ mg/cm² is deposited on the samples. The detailed spraying procedure employed in this study to obtain uniform salt mixture was reported elsewhere in detail (Ref 35). The salt mixture deposition was maintained at ~ 2.5 mg/cm² throughout the study. Isothermal hot corrosion exposure was done for a duration of 1 to 500 h at 800 °C. The procedure to obtain the weight loss or weight gain of the hot corroded samples is described below. Prior to placing the salt mixture-coated samples inside the alumina boat, alumina boat was annealed at 800 °C for 2 h to remove any residual contamination in the boat. Subsequently, two platinum rings were placed inside the alumina boat. The salt mixture-coated sample was placed on these platinum rings inside the alumina boat. This weight of the alumina boat together with platinum rings and the coated sample was measured. After completion of the hot corrosion test, again, the weight of the alumina boat together with platinum rings and the

coated sample was measured. It is important to mention that measuring the weight of the alumina boat together with platinum rings and coated sample ensured that the hot corrosents spalled from the samples were not ignored. The weight loss or gain reported is based on these two measurements taken before and after the hot corrosion test and is an average of two such measurements from two samples at each testing condition. A cautionary note on the interpretation of the weight loss reported in the present study is discussed below.

While samples were taken outside the furnace along with the boat (for measurement) from 800 °C to room temperature after a hot corrosion experiment, a considerable portion of porous oxides and corrosion products would have spalled off from the boat. The weight loss reported here is attributed only to such oxides and compounds spalled off from the boat and volatile compounds. The spalled off oxides from the sample, but inside the boat (minor amount) are not considered as weight loss in the present study. Therefore, the weight loss that is reported here is an underestimation of the actual overall weight loss.

Among the two sets of samples, one set of the samples was extensively used for x-ray diffraction (XRD), SEM, and SEM-EDS studies, and another set of samples was used primarily for EPMA studies. The XRD studies were carried out using an Xpert Pro Analytical Instruments with $\text{Cu-K}\alpha$ radiation. The Xpert High Score Plus software was used to analyze the x-ray peak pattern for peak identification and deconvolution of some of the overlapped XRD peaks. The Raman spectroscopy (Horiba Yvon HR-800 UV He-Ne laser with 632.8 nm wavelength, laser spot size: 0.85 μm acquisition time: 20 s, without filter at 100X) and scanning electron microscopy (FEG-Inspect F of FEI) equipped with energy-dispersive spectroscopy (EDS), and x-ray mapping were used to identify the corrosion products, surface morphology, and elemental distribution on top of the surfaces and as a function of the depth of attack. The other set of samples was used primarily for Electron Probe Micro Analyzer (EPMA-CAMECA SX-100) studies to understand the extent of diffusion of alloying elements and salt elements from the substrate to oxide and salt layers, and vice versa.

3. Results

3.1 Hot Corrosion Kinetic Studies

To evaluate the kinetics of molten salt mixtures with alloying elements of Nimonic263, isothermal hot corrosion tests were done and their influence on oxidation behavior as a function of time is shown in Fig. 1. Weight gain was observed with pure oxidation, whereas weight loss was observed with both 3SM and 3SM-A. Thus, it is clear that three salt mixtures accelerate the oxidation behavior as compared to pure oxidation. In pure oxidation, weight gain occurs due to the formation of oxide layers such as Cr_2O_3 , NiO, CoO, and their spinels.

Weight gain up to 25 h and subsequent weight loss till 500 h were observed in the samples with 3SM. It appears that corrosion product formation dominates over the volatile compound formation up to 25 h and subsequently the formation of volatile compounds dominates over corrosion products till 500 h. However, in contrast, samples coated with 3SM-A exhibit weight loss up to 200 h and then metal loss (weight of the samples after hot corrosion test are less than bare substrate) up to 500 h. It suggests that with 3SM-A, volatile compounds

formation is dominant over corrosion product formation from the beginning, and it becomes more aggressive during 200-500 h. In general, weight loss is attributed to volatile compounds and spallation of oxides. Usually, NaCl breaks down

the oxide layers and form metal chlorides and liberate as volatile compounds and form pits. Further, metal chlorides react with oxygen again to form porous oxides. In the present study, it is apparent that alloying elements of Nimonic263 may form volatile compounds along with metal chlorides and sodium oxychlorides. It is also anticipated that the weight fraction of individual constituents Na_2SO_4 , NaCl , and NaVO_3 plays a major role in hot corrosion. In addition, quantitatively, the weight loss is also more in 3SM-A as compared to 3SM. So, NaCl in 3SM-A can be responsible for more weight loss due to its high weight percentage. More specific reasons and analysis for the weight loss in 3SM and metal loss in 3SM-A condition are explained in the subsequent sections.

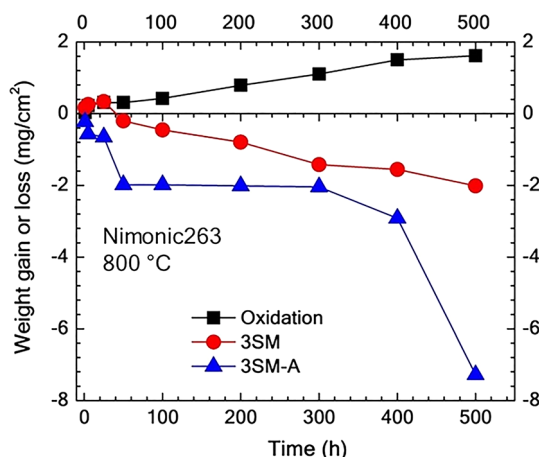


Fig. 1 Isothermal hot corrosion tests on Nimonic263 with and without 3SMs at 800 °C show that 3SM-A is more aggressive than 3SM

3.2 XRD Analysis on Top Surfaces of 3SM and 3SM-A Hot Corroded Samples

The XRD analysis was carried out to identify the corrosion products and volatile compounds that formed at each stage during 5 to 500 h duration of hot corrosion of Nimonic263 with 3SM and 3SM-A. Figure 2(a) and (b) shows the XRD patterns of the hot corroded sample with 3SM for a duration of 5-100 h and for 200-500 h, respectively. Similarly, Fig. 3(a) and (b) displays the XRD patterns of 3SM-A hot corroded samples for a duration of 5-100 h and for 200-500 h, respectively. The

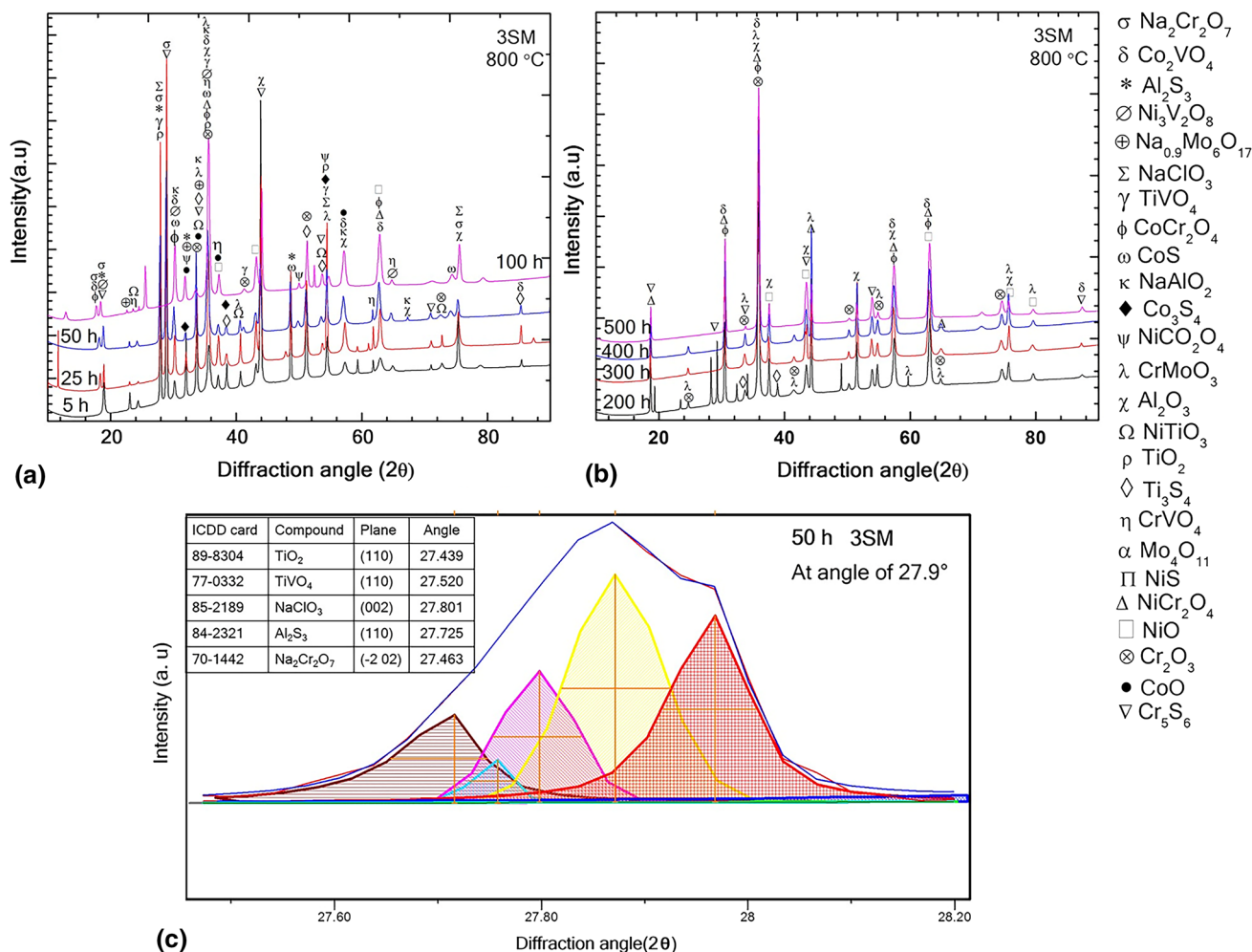


Fig. 2 XRD pattern analysis of Nimonic263 hot corroded at 800 °C with 3SM (a) after exposure for 5-100 h, (b) after 200-500 h, and (c) deconvoluted peaks at 27.9° for 50 h

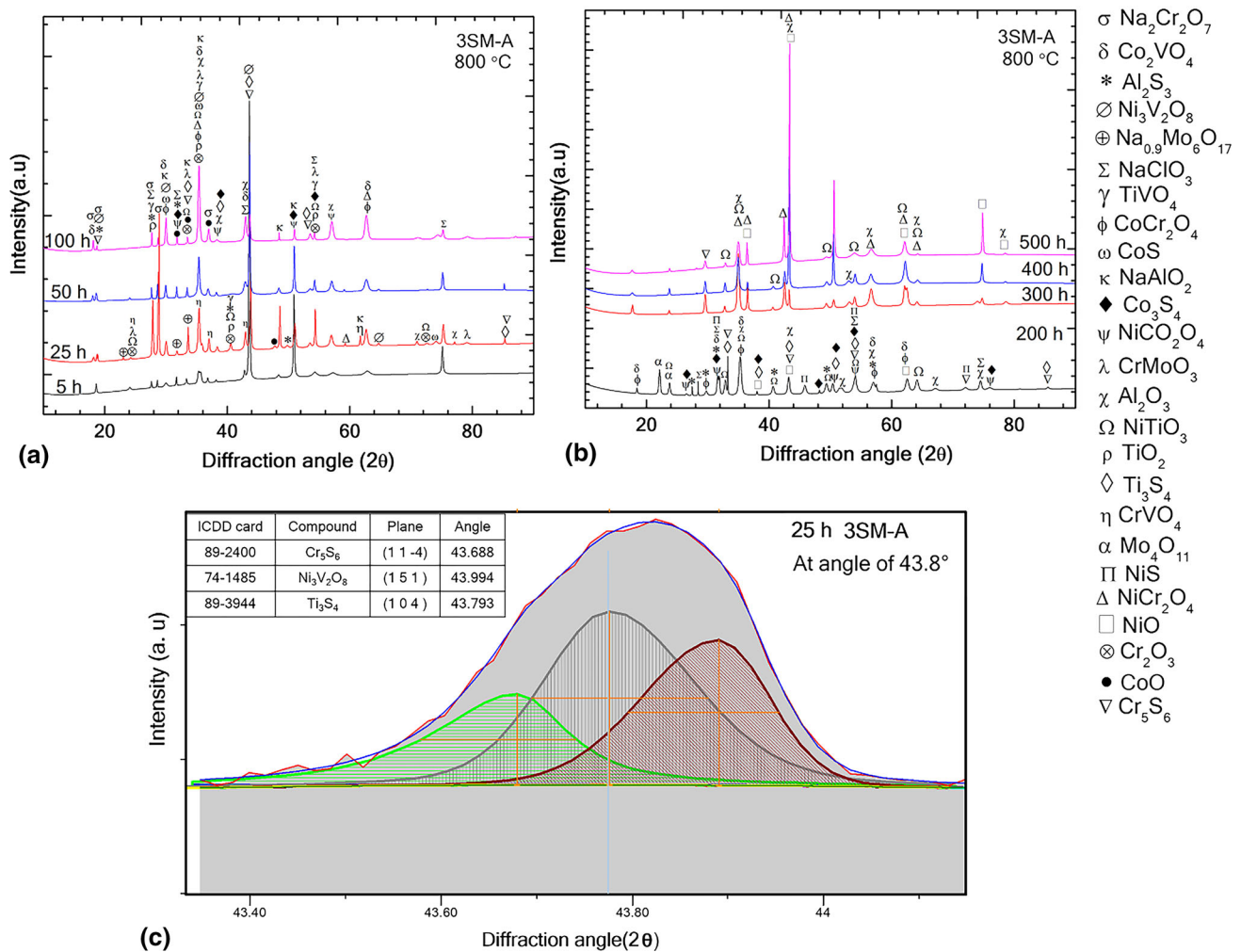


Fig. 3 XRD pattern analysis of Nimonic263 hot corroded at 800 °C with 3SM-A (a) after exposure for 5-100 h, (b) after 200-500 h, and (c) deconvoluted peaks at 43.8° for 25 h

following compounds were observed up to 100 h under both the salt mixtures, namely, Cr-containing compounds: Cr₂O₃, Cr₅S₆, and CrVO₄, Ni-compounds: NiO, NiCo₂O₄, NiCr₂O₄, NiTiO₃, and Ni₃V₂O₈, Ti-compounds: TiO₂, Ti₃S₄, and TiVO₄, Co-compounds: CoO, CoCr₂O₄, CoS, Co₃S₄, and Co₂VO₄, Al-compounds: Al₂O₃ and Al₂S₃, and Na-compounds: Na_{0.9}Mo₆O₁₇, Na₂Cr₂O₇, NaClO₃, and NaAl₂O₄. Also, the CrMoO₃ compound was observed only in 3SM-A but not in 3SM and NiO observed just in 3SM but not in 3SM-A during the first 100 h.

It is understandable from Fig. 2 and 3 that XRD peaks of some of the compounds are overlapped. To ascertain that those peaks belong to the identified compounds, some of the peaks are analyzed by deconvolution method and are shown in Fig. 2(c) and 3(c). Figure 2(c) and 3(c) illustrate the deconvolution of 27.90° peak of 3SM-50 h sample and 43.80° peak of 3SM-A-25 h sample, respectively, showing the various compounds overlapped in those peaks. Table 2 presents all the corrosion products that were characterized by XRD over a duration of 5-100 h, 200-500 h for 3SM and 5-100 h, 200 h, and 300-500 h for 3SM-A at 800 °C.

Among all these compounds, Na₂Cr₂O₇, NaClO₃, and CrMoO₃ are volatile compounds. The weight gain up to 25 h for 3SM is perhaps due to the dominance of vanadate formation

over the liberation of Na₂Cr₂O₇ and NaClO₃, but subsequent weight loss up to 100 h is possibly due to volatile compounds such as Na₂Cr₂O₇ and NaClO₃. Thus, it is understandable that CrMoO₃ is also responsible for weight loss during 200 to 500 h in 3SM condition. Further, in 3SM condition, CrMoO₃ started appearing from 200 to 500 h along with Cr₂O₃, Al₂O₃, CoCr₂O₄, Cr₅S₆, Ti₃S₄, Ni₃V₂O₈, and CrVO₄. In contrast, the CrMoO₃ compound formation in 3SM-A condition leads to weight loss from 1 h of exposure as shown in Fig. 1.

In 3SM-A condition, after 200 h, the formation of NiO, Al₂O₃, CoCr₂O₄, NiCo₂O₄, Al₂S₃, Cr₅S₆, Ti₃S₄, Co₃S₄, NiS, NaClO₃, and Mo₄O₁₁ also was observed. The compound Mo₄O₁₁ is also the contributors for the weight loss at 200 h in 3SM-A condition. NiO, Al₂O₃, NiTiO₃, and NiCo₂O₄ oxides were observed in 3SM-A condition from 300 to 500 h. During air quenching from 800 °C, these porous oxides spalled off from the substrate and fell inside as well as outside the boat due to the lack of adherence to the substrate. Consequently, the metal loss was observed in these samples (Fig. 1).

The spallation regions and pores on the substrate are shown in BSE micrographs of a hot corroded sample of 3SM-A-500 h in the next Section. Perhaps, after the complete consumption of molten salt mixtures, oxygen participation in reactions happens similar to high-temperature oxidation behavior. Therefore, it

indicates that all the alloying elements of Nimonic263 substrate partook in the hot corrosion process under the influence of both salt mixture combinations (3SM and 3SM-A). It also confirms that all the phases Ni-solid solution matrix, Cr₂₃C₆, TiC, and Ni₃Al precipitates of Nimonic263 contribute in accelerating the hot corrosion phenomenon. In contrast, a detailed LTHC hot corrosion study by Mannava et al. (Ref 29) on IN718 with 3SM at 650 °C has shown that Cr, Ni, and Fe elements predominantly participated in the hot corrosion. It appears that the

activity of alloying elements and the extent of molten salts participation in hot corrosion depend mainly on temperature.

Based on the various compounds characterized by XRD analysis, the following two noteworthy points emerge: (a) at 800 °C, 3SM-A is more aggressive than 3SM and (b) the kinetics with 3SM seem to be controlled by the same mechanism till 500 h, whereas with 3SM-A, one type of mechanism operates till 100 h, and subsequently, some other mechanism may be dominant till 500 h.

Table 2 Corrosion products formed during hot corrosion of Nimonic263 with 3SM and 3SM-A at 800 °C

3SM		3SM-A		
5-100 h	200-500 h	5-100 h	200 h	300-500 h
Cr ₂ O ₃	Cr ₂ O ₃	Cr ₂ O ₃		
NiO	NiO		NiO	NiO
TiO ₂		TiO ₂		
CoO	CoO	CoO		
Al ₂ O ₃	Al ₂ O ₃	Al ₂ O ₃	Al ₂ O ₃	Al ₂ O ₃
CoCr ₂ O ₄	CoCr ₂ O ₄	CoCr ₂ O ₄	CoCr ₂ O ₄	
NiCr ₂ O ₄	NiCr ₂ O ₄	NiCr ₂ O ₄		
NiTiO ₃	NiTiO ₃	NiTiO ₃	NiTiO ₃	NiTiO ₃
NiCo ₂ O ₄		NiCo ₂ O ₄	NiCo ₂ O ₄	NiCo ₂ O ₄
CoS	CoS	CoS		
Co ₃ S ₄		Co ₃ S ₄	Co ₃ S ₄	
Cr ₅ S ₆	Cr ₅ S ₆	Cr ₅ S ₆	Cr ₅ S ₆	
Ti ₃ S ₄	Ti ₃ S ₄	Ti ₃ S ₄	Ti ₃ S ₄	
Al ₂ S ₃		Al ₂ S ₃	Al ₂ S ₃	
Na ₂ Cr ₂ O ₇		Na ₂ Cr ₂ O ₇		
NaClO ₃		NaClO ₃	NaClO ₃	
NaAlO ₂		NaAlO ₂	NaAlO ₂	
Na _{0.9} Mo ₆ O ₁₇		Na _{0.9} Mo ₆ O ₁₇		
CrVO ₄	CrVO ₄	CrVO ₄		
Ni ₃ V ₂ O ₈	Ni ₃ V ₂ O ₈	Ni ₃ V ₂ O ₈		
TiVO ₄		TiVO ₄		
Co ₂ VO ₄	Co ₂ VO ₄	Co ₂ VO ₄		
	CrMoO ₃	CrMoO ₃		
			NiS	
			Mo ₄ O ₁₁	

3.3 Raman Analysis on Top Surfaces of 3SM and 3SM-A Hot Corroded Samples

The XRD analysis has its limitations. For example, XRD cannot detect the compounds when vol.% of the compounds are insubstantial (< 5%). Thus, the Raman spectroscopy analysis was done on the top surfaces of hot corroded samples in order to identify such corrosion products which cannot be detected by XRD. Figure 4 shows the Raman spectroscopy analysis of hot corroded samples of Nimonic263 with 3SM (Fig. 4a) and 3SM-A (Fig. 4b). The oxides, spinels, and sulfides were observed in both conditions, and vanadates were observed only in 3SM condition. The wave numbers for Cr₂O₃, CoCr₂O₄, NiS, V₂O₅, Ni₃(VO₄)₃, TiVO₄, and CrVO₄ phases are 614, 452, 142 995, 861, 640, and 773 cm⁻¹, respectively (Ref 36-40). The peaks corresponding to Co₃O₄ were observed at the wave numbers of 194 and 521 cm⁻¹ (Ref 41) and for the NiCr₂O₄ compound were identified at 508 and 676 cm⁻¹ (Ref 36). Similarly, the wave numbers of 303, 710, 822, and 954 cm⁻¹ corresponding to AlVO₄ peaks (Ref 39) and peaks for Na₂SO₄ were observed at the wave numbers of 976, 1090, 1108, 1130, and 1196 cm⁻¹ (Ref 42, 43).

It is important to note that Co₃O₄, V₂O₅, NiS, Ni₃(VO₄)₃, and Na₂SO₄ compounds were not detected in XRD analysis, but only observed via Raman analysis. Besides, Na₂SO₄ and V₂O₅ were observed just up to 400 h in 3SM condition (Fig. 4a) but not in 3SM-A. This critical observation from Raman analysis suggests that Na₂SO₄ and V₂O₅ participate in hot corrosion process till 400 h with the 3SM condition. Consequently, vanadates were observed till 500 h in 3SM (Fig. 2b). Similarly, V₂O₅ was observed up to 25 h and vanadate products appeared till 100 h with 3SM-A (Fig. 3b and 4b). Further, with 3SM-A, vanadate products were not observed

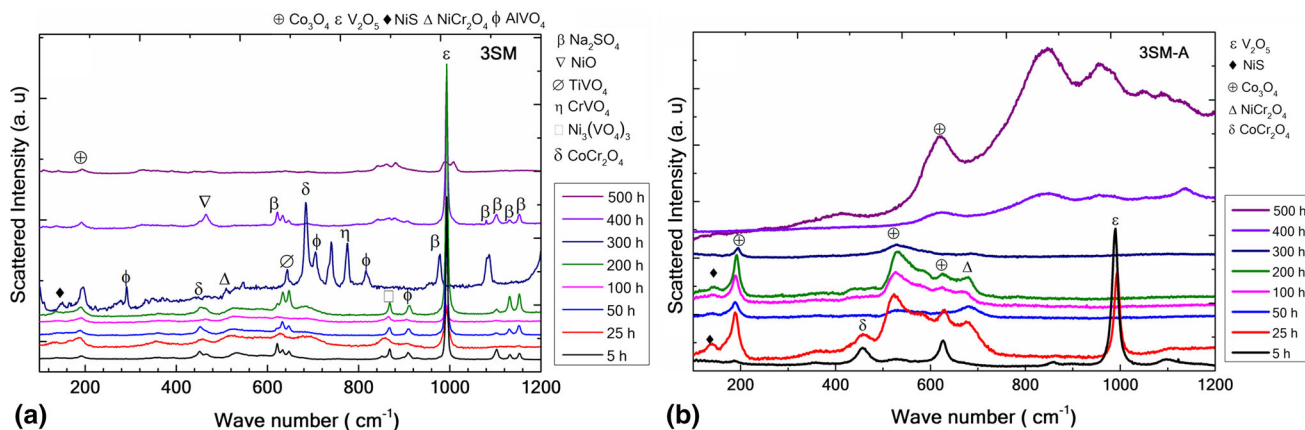


Fig. 4 Raman spectroscopy analysis of Nimonic263 hot corroded samples with (a) 3SM during 5-500 h and (b) 3SM-A, after exposure for 5-500 h, suggesting that Na₂SO₄ and V₂O₅ prevail till 400 h with 3SM, and new corrosion products did not form with 3SM-A during 300-500 h

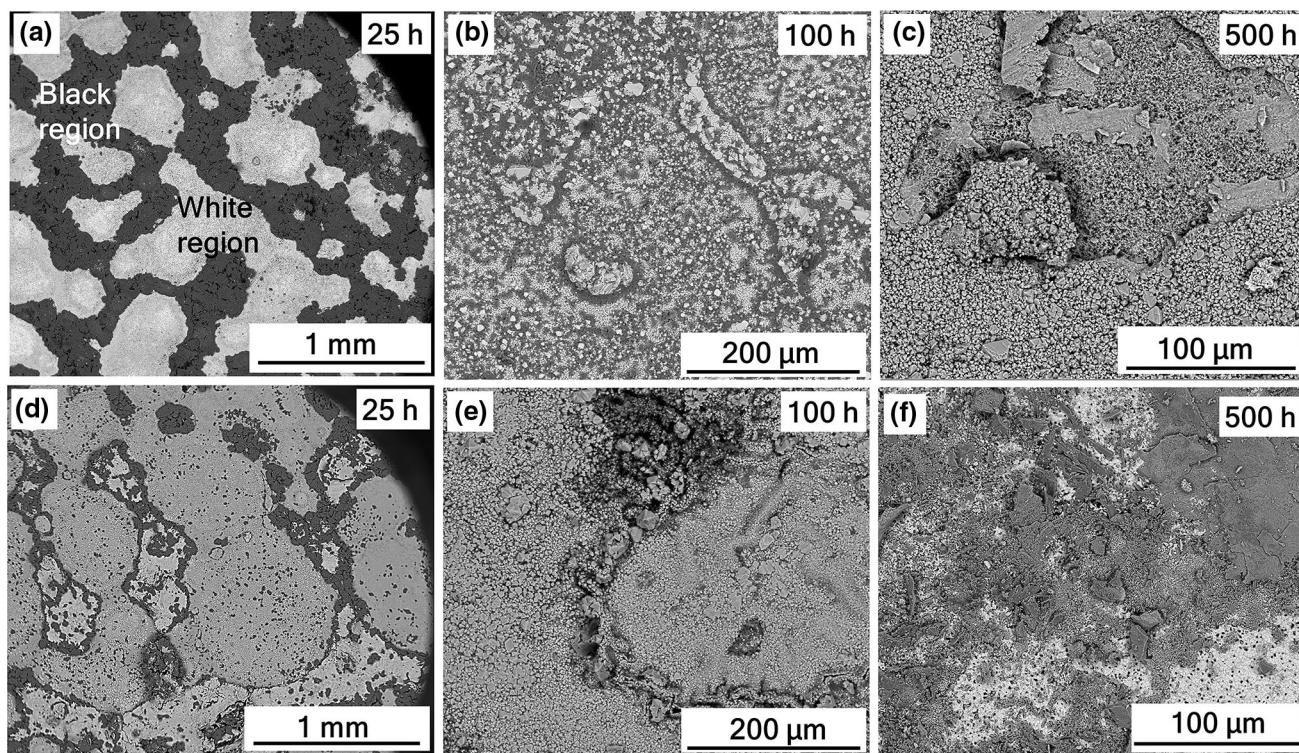


Fig. 5 The BSE-SEM micrographs of Nimonic263 superalloy coated with 3SM and hot corroded at 800 °C for (a) 25 h, (b) 100 h, and (c) 500 h and with 3SM-A for (d) 25 h, (e) 100 h, and (f) 500 h. The extent of hot corrosion acceleration with increasing exposure is illustrated

Table 3 EDS analysis on the top surface of 25-h hot corroded sample with 3SM

Elemental composition (wt.%)	3SM 25 h								
	Ni	Cr	Co	Mo	Ti	Al	Na	S	V
White region	16.10	35.85	12.50	1.58	2.39	0.39	10.22	0.91	3.18
Black region	1.11	3.67	0.91	20.74	0.82	0.19	29.61	21.93	0.6

in both XRD and Raman after 100 h, and only oxides are observed from 300 to 500 h in XRD analysis (Fig. 3b and 4b).

3.4 Microstructural Characterization of Top Surfaces of Hot Corroded Samples with 3SM and 3SM-A

Figure 5 shows the BSE microstructures of the top surfaces of hot corroded samples of 3SM (Fig. 5a, b and c for 25 h, 100 h, and 500 h, respectively) and 3SM-A (Fig. 5d, e and f for 25 h, 100 h and 500 h, respectively). From Fig. 5(a) of 3SM, there are two contrasting regions of white (3SM completely reacted with alloy) and black (unreacted 3SM). The corresponding EDS analysis of 25 h sample is presented in Table 3. The weight percentages reported here are from an average of two independent spot analyses in each region. It is clear from Table 3 that white region consists of higher weight percentage of Ni, Cr, Co, Ti, and V (major alloying elements in Nimonic263) and the lower weight percentage of Na, S, and Mo. In contrast, the black region shows the lower percentage of Ni, Cr, Co, Ti, and V, but higher weight percentage of Na, S, and Mo.

It suggests that Na_2SO_4 remains on the top of the surface of the samples up to 25 h and NaVO_3 completely participates in

hot corrosion. This observation also confirms that in both 3SMs, the constituents start melting at the interface between the salt mixture and Nimonic263 substrate due to a lower oxygen activity. However, in 100 h (Fig. 5b), the signs of Na_2SO_4 on the top of the surface are not visible. Therefore, it implies that all constituents of 3SM completely go into the molten state after 25 h and react with alloying elements of the Nimonic263 alloy. However, the weight loss shown after 25 h (Fig. 1) might be due to the evaporation of volatile compounds such as $\text{Na}_2\text{Cr}_2\text{O}_7$, NaClO_3 as characterized in Fig. 2. Further, detachment between Nimonic263 and corrosion products was observed in 500 h of 3SM sample (Fig. 5c), which arises due to the spallation of corrosion products. These corrosion products might be porous oxides

In contrast, on 3SM-A hot corroded samples, there was no signature of residual salt deposition from 25 h onwards (Fig. 5d, e and f). It suggests that molten salts of 3SM-A completely participate in hot corrosion reactions from the beginning of the exposure at 800 °C. As mentioned earlier based on Fig. 2 and 3, the evaporation of volatile compounds $\text{Na}_2\text{Cr}_2\text{O}_7$, CrMoO_3 may also contribute toward weight loss till 100 h and then Mo_4O_{11} also aids toward the weight loss till 200 h. During cooling, these corrosion products spalled off

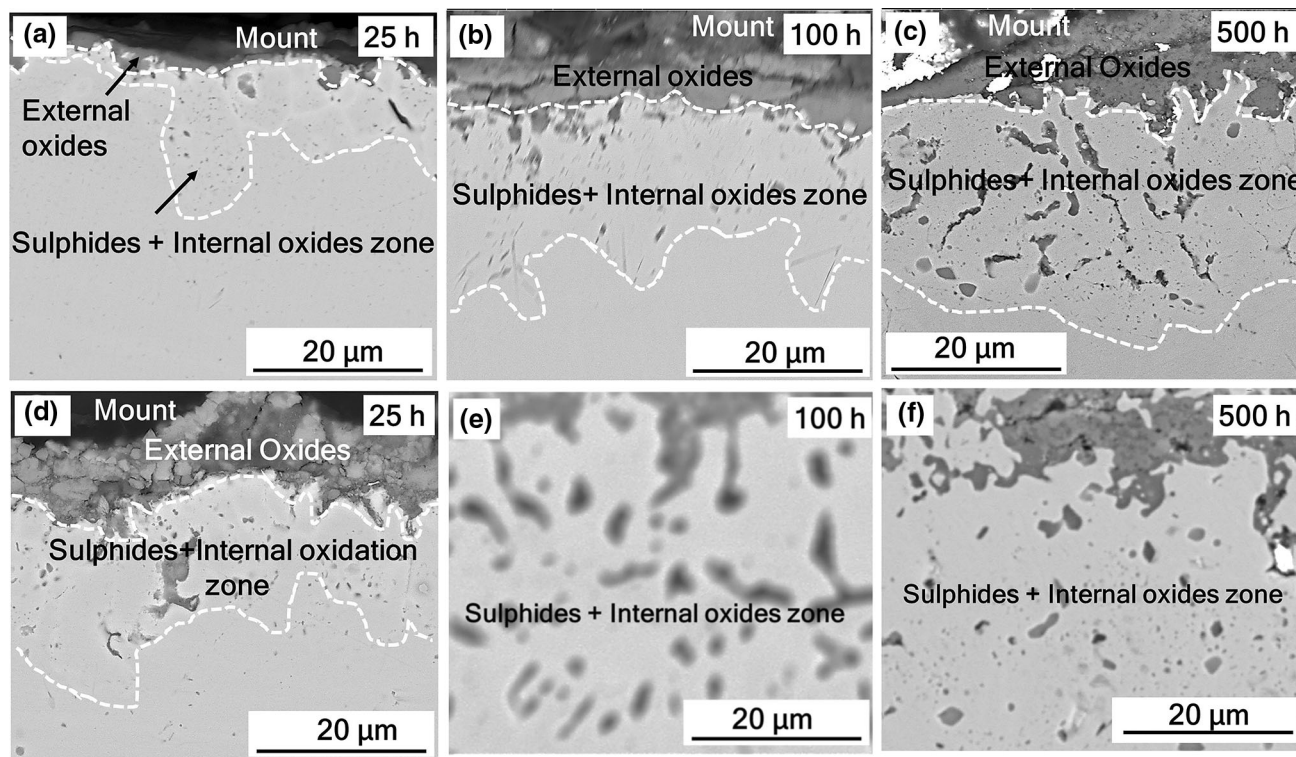


Fig. 6 Cross-sectional BSE-SEM micrographs of Nimonic263 superalloy with 3SM after (a) 25 h, (b) 100 h and (c) 500 h and with 3SM-A for (d) 25 h, (e) 100 h, and (f) 500 h of hot corrosion duration at 800 °C displaying the external oxides and sulfides plus internal oxidation zone. It also shows the increase in these regions as exposure duration increases

from the surface, and the top surface appears as a bare substrate with pores as well as with loosely adhered corrosion products (Fig. 5c), which lead to excessive weight loss as displayed in Fig. 1 (300-500 h). So, excessive weight loss is an indication of the formation of volatile compounds of alloying elements Mo and Cr of Nimonic263 and spallation of corrosion products during hot corrosion.

3.5 Cross-sectional Microstructural Characterization of Hot Corroded Samples with 3SM and 3SM-A

In order to characterize the extent of the influence of various salt elements underneath the coating and into the Nimonic263 substrate, a detailed microstructural characterization was carried out on cross sections of both 3SM and 3SM-A hot corroded samples. Figure 6 illustrates the cross-sectional BSE microstructures of hot corroded samples with 3SM (Fig. 6a, b and c for 25 h, 100 h and 500 h, respectively) and with 3SM-A (Fig. 6d, e and f for 25 h, 100 h and 500 h, respectively). From Fig. 6, it is clear that the molten salt attack is not uniform, and preferential attack is present along grain boundaries than the interior of the grains. It suggests that grain boundary precipitates such as Cr_{23}C_6 and TiC are more prone to hot corrosion than the matrix.

Broadly, both 3SM and 3SM-A hot corroded samples show two zones. The top one is external oxide zone, and beneath one is sulfides plus internal oxides zone, while this is an exception for 100 h and 500 h of 3SM-A condition (Fig. 6e and f) in which the external oxide zone is not present. With 3SM, during 25 to 500 h of hot corrosion duration, sulfides plus internal oxides zone increases. In contrast, with 3SM-A sample, sulfides plus internal oxides zone increases up to 100 h, and then, it was

constant up to 500 h. For 25 and 100 h, sulfides plus internal oxides zone doubled in 3SM-A as compared to that of 3SM. It indicates that the attack by 3SM-A is more aggressive than by 3SM and it can be possibly attributed to more amount of NaCl present in 3SM-A than in 3SM.

Mannava et al. (Ref 29) conducted a detailed hot corrosion study on IN718 with 3SM at 650 °C and reported that salts of 3SM uniformly attack and form Cr- depletion layer, and there was no participation of Ni_3Al precipitates in hot corrosion. However, the present study on Nimonic263 with 3SM at 800 °C shows more aggressive behavior. It is clear that besides Cr, other alloying elements such as Al (formation of Al_2O_3 , Al_2S_3 , and NaAlO_2 compounds), Ti (TiO_2 and Ti_3S_4 compound) and Mo (Mo_4O_{11} compound) also participate more actively in hot corrosion at 800 °C. Clearly, as the temperature increases, salts are more aggressively reacted with alloying elements of superalloy and participated in hot corrosion.

3.6 EPMA/x-ray Mapping and Line Scan Analysis of Cross-sectional Hot Corroded Samples

To evaluate the extent of the diffusion of salt elements into the substrate and alloying elements on to the surface, EPMA/x-ray mapping was done on cross sections of the hot corroded samples. It is necessary to note that the x-ray mapping was captured from the external layer into the Nimonic263 substrate, and the mount region was omitted since there was excessive charging while imaging along with mount region. The EPMA mapping of a 3SM hot corroded sample of 25, 100, and 500 h is shown in Fig. 7(a), (b), and (c), respectively. Similarly, for 3SM-A hot corroded samples, EPMA mapping of 25, 100, and 500 h is shown in Fig. 8(a), (b) and (c), respectively.

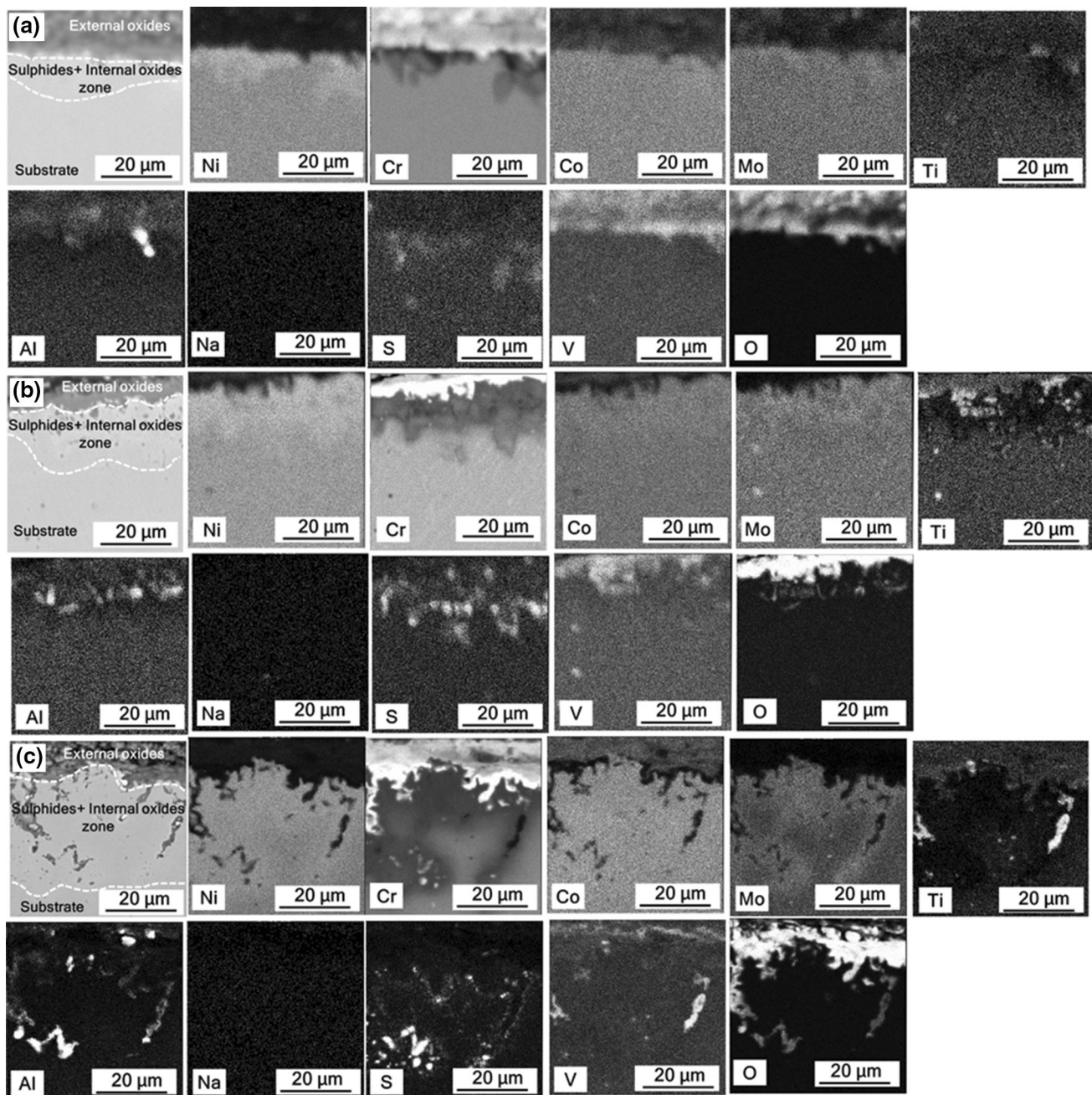


Fig. 7 EPMA mapping of Nimonic263 coated with 3SM and hot corroded at 800 °C as a function of hot corrosion duration (a) 25 h, (b) 100 h, and (c) 500 h at 800 °C showing the diffusion of alloying elements into the surface and vice versa. Cr diffusion and S penetration into the substrate increase as oxidation duration increases

An overarching observation from Fig. 7 and 8 is that the attack of both salt mixtures is not uniform and is consistent with the observations from Fig. 6. Moreover, hot corroded samples with 3SM-A had undergone more degradation than 3SM. The Na does not show any preferential diffusion, suggesting that Na completely react with Cr and Mo and form volatile compounds such as $\text{Na}_2\text{Cr}_2\text{O}_7$ and $\text{Na}_{0.9}\text{Mo}_6\text{O}_{17}$ as evident from Fig. 2 and 3. Although, Fig. 2, 3 and 4 show the formation of Ni, Co, V, and Mo compounds; these elements do not display any significant diffusion and participation in hot corrosion up to 25 h with both salt mixture combinations (Fig. 7a and 8a). However, after 100 h and 500 h, the Ni, Co, V, and Mo show significant depletion at specific small regions under both

conditions (Fig. 7b, c, and 8b, c). Thus, Ni, Co, and Mo diffusing out after 25 h to contribute to hot corrosion.

Besides, in 25 h sample, it was observed that Cr is depleted between external oxide and sulfides plus internal oxides zones in 3SM sample, and some spots and regions are Cr-depleted within the sulfides plus internal oxides zone 3SM-A. In 100 h samples, Cr is entirely (uniform) depleted in 3SM condition, whereas Cr depletion is more pronounced in sulfides plus internal oxides zone in 3SM-A condition. Further, after 500 h, the Cr depletion is almost similar to that of 100 h and few other regions become richer in Cr under both salt mixture conditions. Thus, it suggests that Cr is diffusing out more under 3SM-A condition than under 3SM.

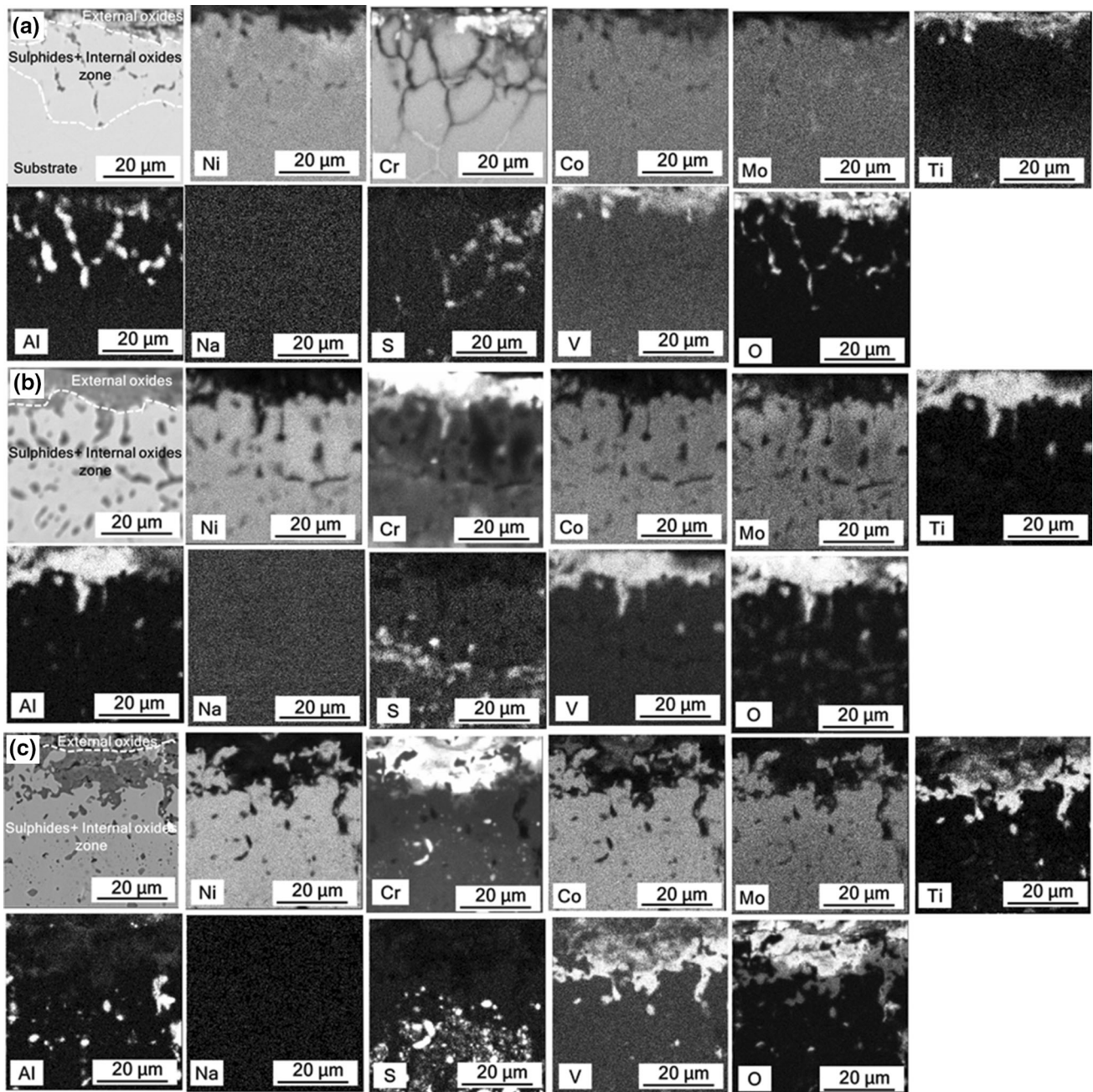


Fig. 8 EPMA mapping of Nimonic263 coated with 3SM-A and hot corroded at 800 °C, as a function of the duration of exposure (a) 25 h, (b) 100 h, and (c) 500 h, indicating the diffusion of alloying elements into the surface and vice versa. Cr and Ti diffuse onto surface, and S penetration into the substrate increases as hot corrosion duration increases

After 25 h, preferential diffusion of Al and Ti was not observed in 3SM condition, whereas diffusion of these two elements was observed in 3SM-A condition and is richer in external oxides region. It suggests that Al and Ti are more aggressively participating in hot corrosion under 3SM-A condition. Further, under both salt mixture conditions, it was observed that Al and Ti are more abundant in sulfides plus internal oxides zone than in oxide region at a longer duration of 100 h and 500 h. It was also observed that O is richer in external oxide zone in 25 h and 100 h samples in 3SM condition, whereas O is richer in both external oxide region and in sulfides plus internal oxides zones in 500 h sample of 3SM condition and also in 25, 100, and 500 h of 3SM-A condition.

Further, it was found that as the hot corrosion exposure increases, S penetration also increases except for 25 h sample in 3SM condition. Most of these observations together suggest that the constituents of 3SM-A are much more aggressive in degrading the Nimonic263 at 800 °C than 3SM.

Figure 9 and 10 show the line scan analysis of a cross section of 3SM (Fig. 9a, b, c, d, e, f, g, h and i) and 3SM-A (Fig. 10a, b, c, d, e, f, g, h and i) hot corroded samples at various hot corrosion durations of 25 h, 100 h, and 500 h. The line scanning was done into the substrate from the top side of the coating. It is evident from these line scan analyses that Cr and O actively participated in hot corrosion as oxidation time increases under both salt mixture conditions. For 100 h, Al, Ni,

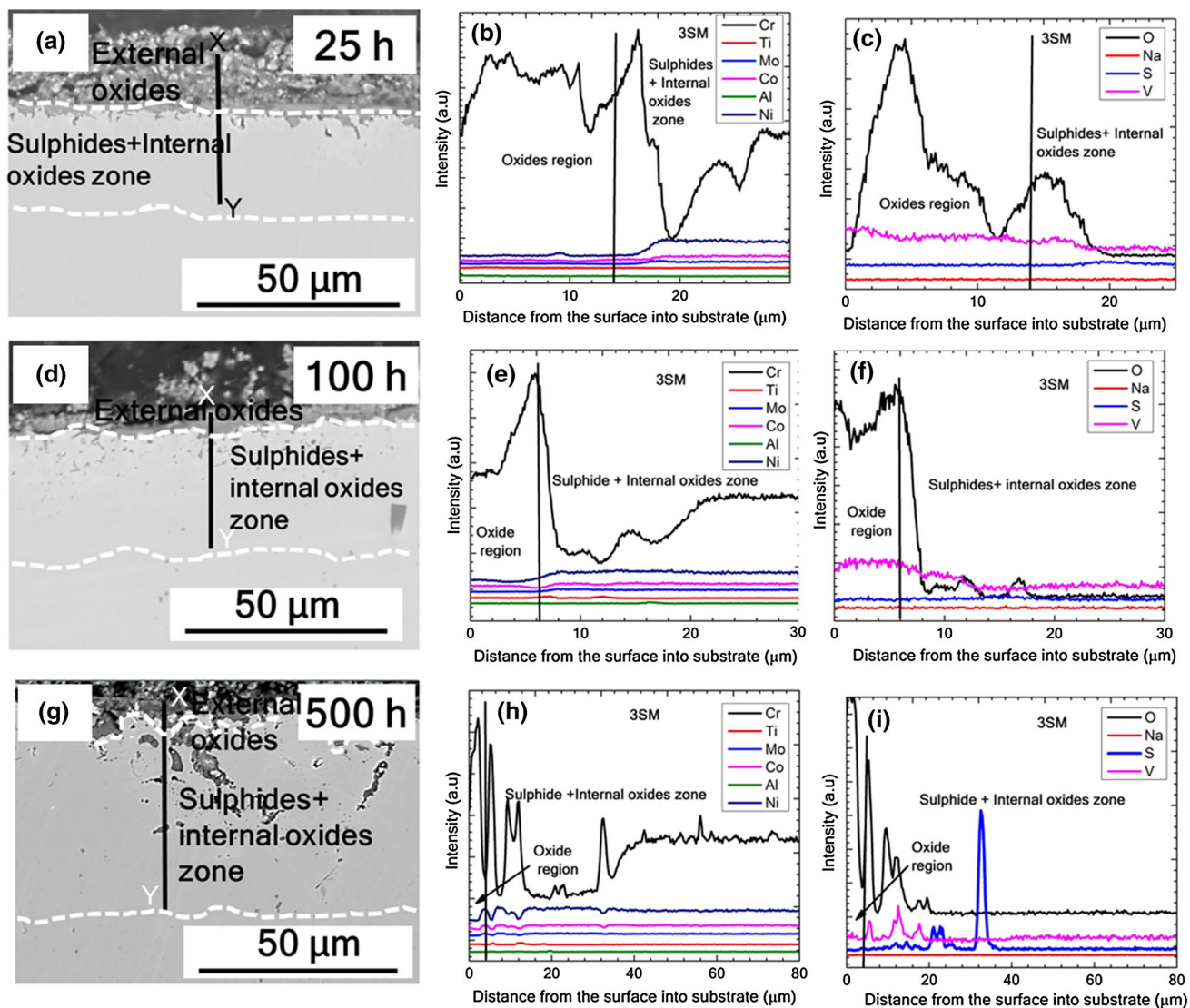


Fig. 9 EPMA line scan analysis of Nimonic263 with 3SM after hot corrosion at 800 °C for (a-c) 25 h, (d-f) 100 h, and (g-i) 500 h at 800 °C. (Line scan starts at X point from the surface into the substrate up to Y point.) This analysis suggests that Cr diffuses out onto the surface, and S and O penetrate the substrate

Mo, Co, and Ti elements show some variation from top to the interior of the substrate under the 3SM-A condition as compared with 3SM. Besides, V and S also show a significant difference under 3SM-A condition than under 3SM. Thus, all these substantiating observations suggest that all alloying elements participate in hot corrosion more under the 3SM-A condition as compared to that under 3SM condition. These observations are also in good agreement with detailed XRD analysis (Fig. 2 and 3), BSE microstructural characterization (Fig. 5 and 6), and EPMA analysis (Fig. 7 and 8).

For 500 h, sulfur shows more penetration along with O and V under both conditions and that can be attributed to increasing of sulfides plus internal oxides zone as the oxidation duration increases (Fig. 6). The Na does not show any variation in both conditions from top of the coating to interior of the substrate. It suggests that only anions such as O^{2-} , SO_4^{2-} , and VO_3^- penetrate the substrate. From an overall EPMA analysis, it is clear that all alloying elements and phases of Nimonic263 superalloy participate actively in hot corrosion. Moreover, active participation of grain boundary precipitates and Ni_3Al

precipitates leads to accelerating hot corrosion under both 3SM and 3SM-A conditions.

The above sections have brought out the crucial observations and interpretations from XRD, Raman spectroscopy, BSE-SEM, and EPMA analyses. Now, based on the above observations and analysis, the following two sections concentrate on explaining the plausible hot corrosion mechanism at 800 °C in Nimonic263 under the influence of salt mixture combinations (3SM and 3SM-A) mimicking the marine-like environment conditions.

4. Discussion

4.1 A Plausible Hot Corrosion Mechanism of Nimonic263 with Na_2SO_4 - $NaCl$ - $NaVO_3$ at 800 °C

A plausible stage-by-stage hot corrosion mechanism of 3SM and 3SM-A with Nimonic263 at 800 °C is illustrated schematically in Fig. 11. If the ternary phase diagram of Na_2SO_4 - $NaCl$ -

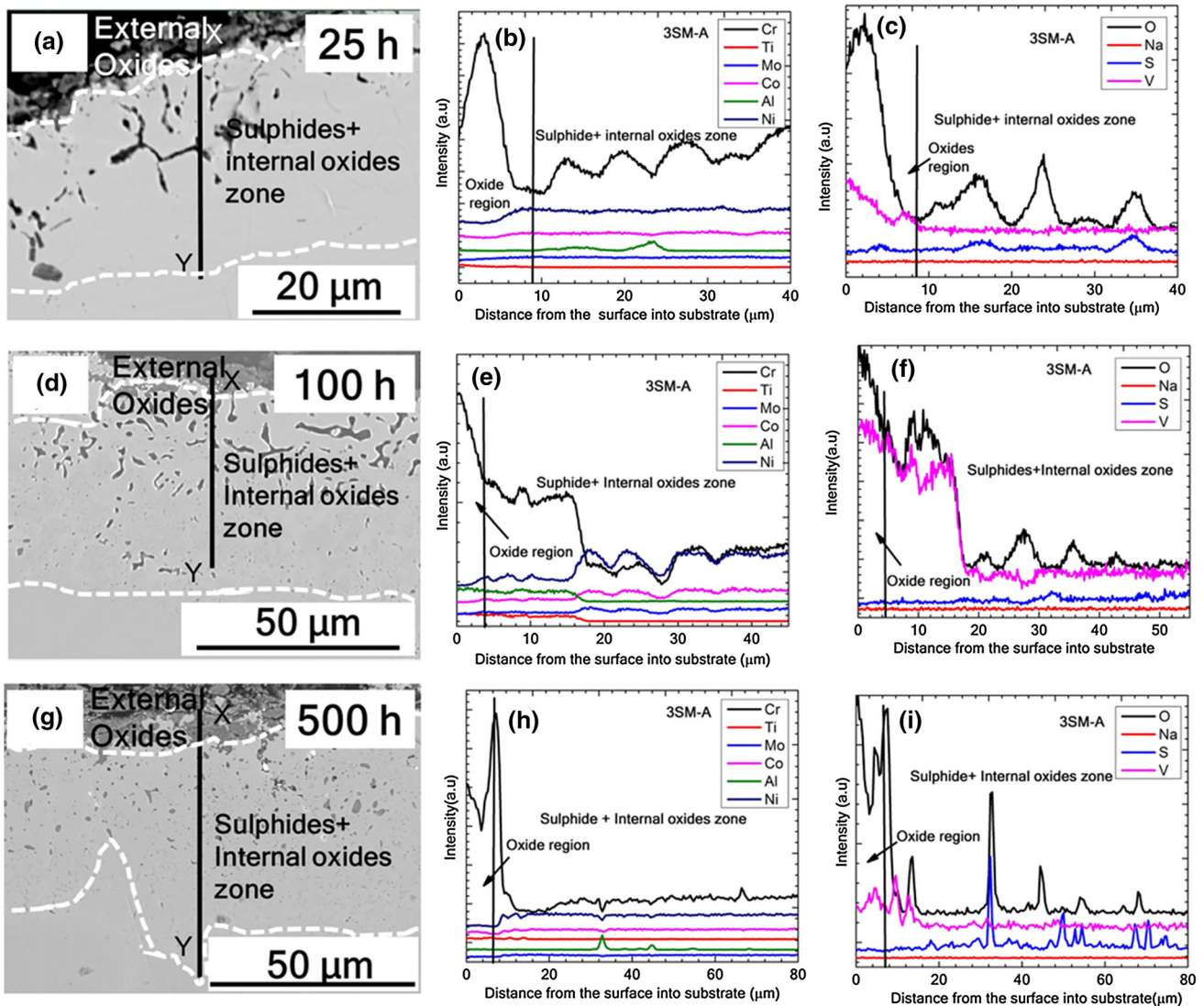


Fig. 10 EPMA line scan analysis of Nimonic263 with 3SM-A as a function of hot corrosion exposure for (a-c) 25 h, (d-f) 100 h, and (g-i) 500 h at 800 °C. (Line scan starts at X point from the surface into the substrate up to Y point.) The penetration of S, V, and O into the substrate is clearly illustrated

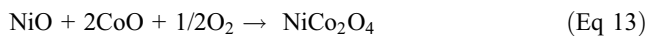
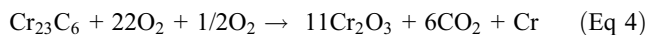
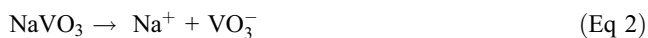
NaVO₃ salts is available, it would have been ideal to predict accurately. However, a detailed literature survey suggests an estimated ternary diagram for certain compositions by Ghosh and Raghavan (Ref 44). Unfortunately, this referred article also does not have definite information on the 3 salt compositions 3SM and 3SM-A of the present study. Therefore, the analysis presented here is based on the binary phase diagrams of Na₂SO₄-NaVO₃ and Na₂SO₄-NaCl (Fig. A1 and A2 are the binary phase diagrams of Na₂SO₄-NaVO₃ and Na₂SO₄-NaCl, respectively, which are shown in supplementary materials section) which were also referred by Ghosh and Raghavan (Ref 44).

When 3SM and 3SM-A reach 800 °C, NaVO₃, NaCl, and Na₂SO₄ constituents start to go into molten state and then become as ions through reactions (1), (2) and (3) as shown in Stage I of Fig. 11, which is also confirmed through binary phase diagrams of Na₂SO₄-NaCl and Na₂SO₄-NaVO₃. Subsequent reaction of these ions with Nimonic263 alloy depends on the activity of Na⁺, VO₃⁻, Cl⁻, and SO₄²⁻ ions. Sidky and Hocking (Ref 45) worked on hot corrosion behavior of Ni-base

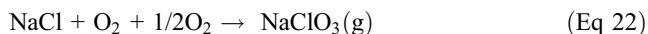
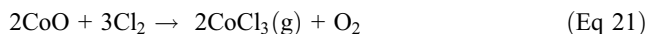
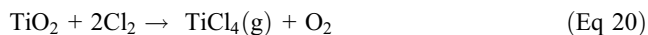
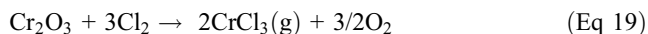
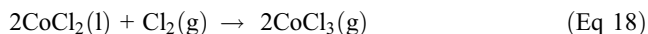
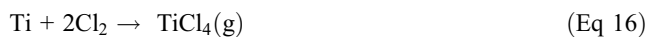
ternary alloys and superalloys with different salt mixture combinations of Na₂SO₄/NaVO₃ in the temperature of 630-900 °C and reported that VO₃⁻ ions activity is faster than SO₄²⁻. Thus, it is clear that at 800 °C, the activity of VO₃⁻ and Cl⁻ ions is faster as compared to that of SO₄²⁻ ions, and thus, VO₃⁻ and Cl⁻ ions are participating more with Nimonic263. Instantaneously, there is a chance for oxygen to diffuse into the substrate and react with Cr₂₃C₆, TiC, Ni₃Al precipitates in Nimonic263 alloy and elements such as Cr, Co, and Ni try to form corresponding oxides via reaction (4) to (9) as shown in Stage I of Fig. 11. Subsequently, spinel compounds also form via reaction (10) to (13) except (12). In some localized regions, Ni₃Al also turns into NiO and Al₂O₃ (reaction (14)). Although all oxides and spinel compounds were observed from XRD analysis for 5 h (Fig. 2a and 3a), oxides Co₃O₄, Cr₂O₃, NiCr₂O₄, and TiO₂ confirmed through Raman spectroscopy analysis (Fig. 12) for 1 h suggest that alloying elements participate in hot corrosion.

At the same time, SO₄²⁻ (reaction (3)) ions turn into SO₃ and O²⁻ ions, as shown in reaction (15), which takes place in

Stage I of Fig. 11 in 3SM-A. Figure 13 shows the Raman spectroscopy analysis of the influence of heating on 3SM and 3SM-A salt mixtures without Nimonic263 at 800 °C for 1 h. It is interesting to note that 3SM-A salt mixtures go into a molten state much faster than that of 3SM. Thus, it is more probable that SO₃ liberation takes place in 3SM-A condition.

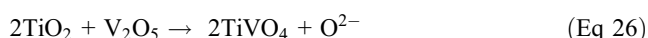
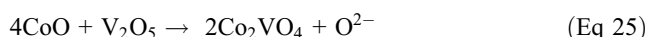
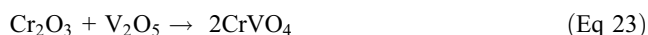


In parallel, there are three possibilities for Cl⁻ (reaction (1)) to participate during hot corrosion. The first possibility is that Cl⁻ ions react with alloying elements such as Ti and Co and form corresponding metal chlorides TiCl₄ and CoCl₃ as shown in reaction (16-18). The second one is that oxides react with Cl₂ and form corresponding chlorides (reactions from (19) to (21)). The third possibility is that NaCl reacts with oxygen and forms sodium oxy-chlorates such as NaClO₂, NaClO₃, and NaClO₄ (reaction (22)).

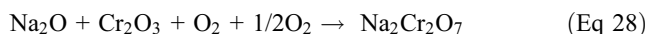


Reactions (16-22) are shown in Stage II of Fig. 11 in both conditions. Subsequently, these chlorides liberate as gases, and they will act as pits which are shown in the cross-sectional microstructures of both 3SM and 3SM-A (Fig. 6). The standard free energy formation of chlorides and oxides at 800 °C is presented in Table 4 (Ref 46). Based on the free energy formation of chlorides and oxides (Table 4), it is evident that Ti and Cr form chlorides and oxides faster (spontaneously) than Co and Ni. It is interesting to note that the similar observation was also observed by Gurrappa (Ref 21) and Tsuar et al. (Ref 47) in CM247LC alloy and 310 stainless steel with different salt mixtures of Na₂SO₄ and NaCl at 900 °C and 750 °C, respectively.

Simultaneously, VO₃⁻ (reaction (2)) turns into V₂O₅ and reacts with Cr₂O₃, NiO, CoO, TiO₂, and Al₂O₃ oxides and forms corresponding CrVO₄, Ni₃V₂O₈, Co₂VO₄, TiVO₄, and AlVO₄ vanadates via reactions (23-27) (Stage II of Fig. 11). It is important to note that all these vanadates were observed in the XRD pattern of hot corroded samples of 3SM and 3SM-A (Fig. 2 and 3).



The formation of Ti and Co vanadates leads to alloy induced acidic fluxing. Concurrently, Na⁺ ions react with surrounding oxygen and form Na₂O, and subsequently, Na₂O reacts with Cr and O or Cr₂O₃ and forms Na₂CrO₄. The Na₂CrO₄ appears as yellow color throughout the boat as was observed in our experiments. Further, Na₂O reacts with Cr and O or Cr₂O₃ and forms Na₂Cr₂O₇ (reaction (28)) that evaporates which was also observed by Rapp (Ref 48) from studies of solubilities of different oxides in Na₂SO₄ at 900 °C. Besides, Na₂O reacts with Mo and O, and Al₂O₃ forms sodium molybdate (Na_{0.9}Mo₆O₉) and NaAlO₂ (reaction (29)) compounds.



From the above reactions, it is clear that oxygen activity is more in localized regions. Subsequently, to attain the equilibrium Cr₂O₃, NiO and Al₂O₃ react with O²⁻ ions and form corresponding chromate, nicklate, and aluminates via reactions (30-32), which leads to basic fluxing and also was observed by Goebel et al. (Ref 7, 8). These reactions are shown in Stage II of Fig. 11 for both conditions of 3SM and 3SM-A. Consequently, SO₂ activity will be more in localized regions. There are two ways to get equilibrium: (i) CoO and TiO₂ dissociate into corresponding cations and O²⁻ ions by acidic fluxing and follow reactions (34 and 35).



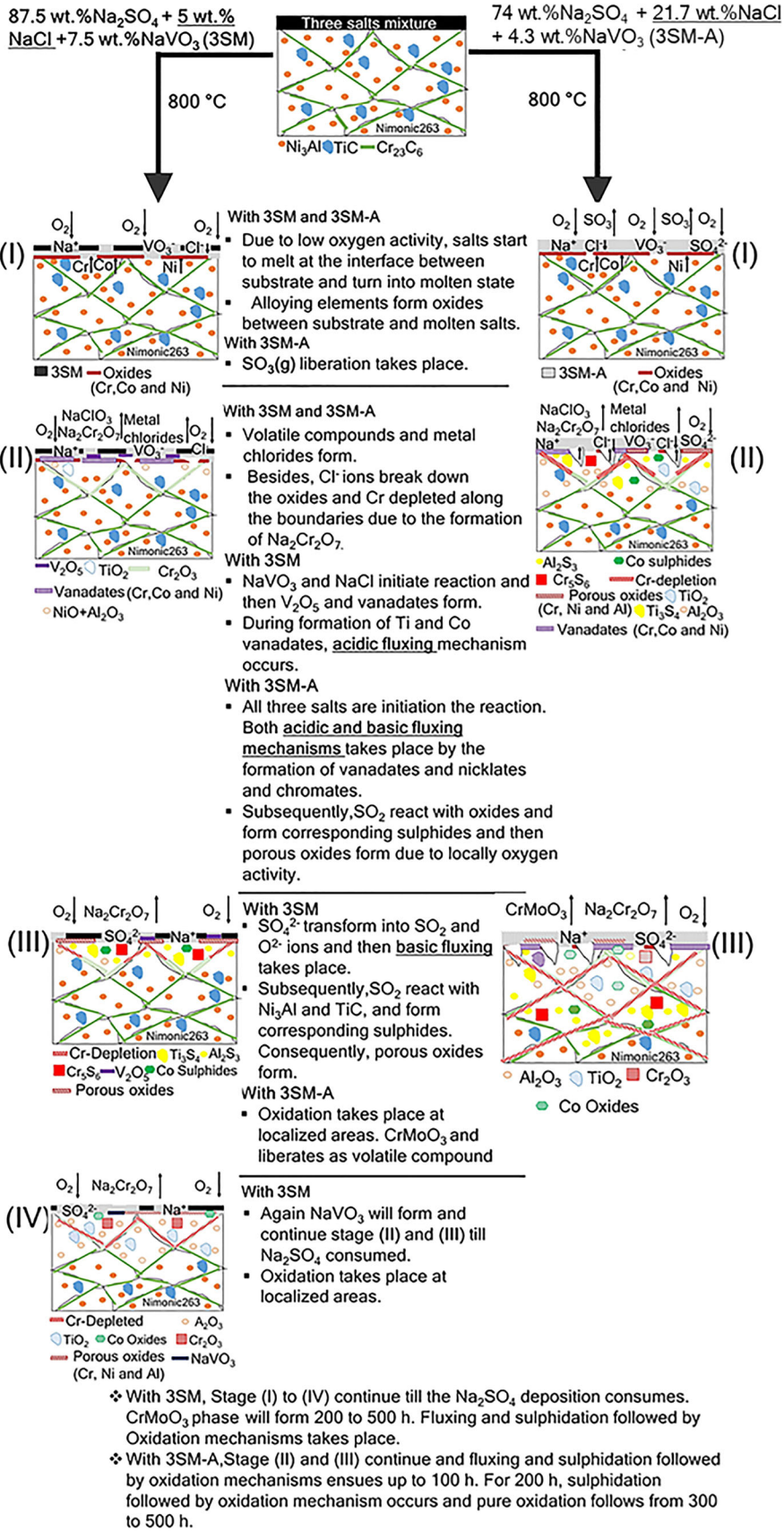


Fig. 11 Schematic diagram showing a plausible hot corrosion mechanism of Nimonic263 with 3SM and 3SM-A mixture coats

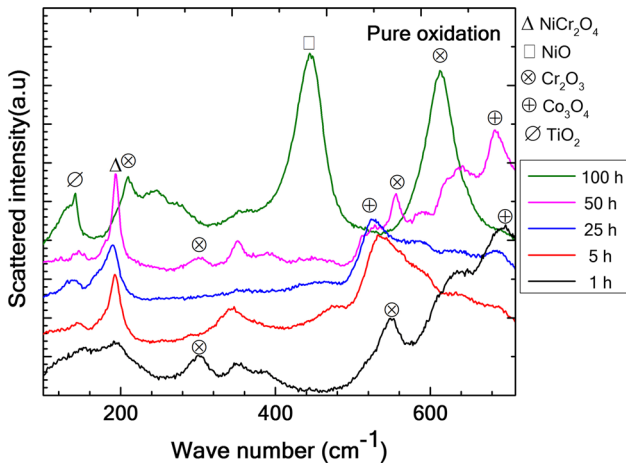


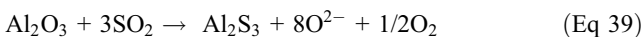
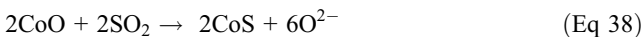
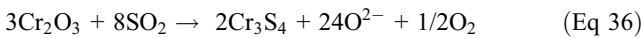
Fig. 12 Raman spectroscopy analysis of Nimonic263 annealed at 800 °C without salt mixtures (pure oxidation) as a function of exposure, showing the formation of oxides from 1 h



Further, SO_4^{2-} ions can form as SO_2 as in reaction (33)



(ii) Oxides react SO_2 and form corresponding sulfides through sulfidation and which are shown in reactions (36-39). This kind of reaction sequence was observed in Ni-Cr-X ternary alloys at 1000 °C with Na_2SO_4 by Seybolt (Ref 4). These compounds are shown in Stage III and Stage II of Fig. 11.



Successively, localized O^{2-} ions activity will be more and again form corresponding oxides through oxidation as shown in Stage IV of Fig. 11. Subsequently, SO_2 will be more in localized regions, and then, again sulfidation takes place. Concurrently, due to the formation of pits, vanadates and volatile compounds at the substrate-oxides interface, there is a chance for oxygen to diffuse into the substrate and react with Cr_{23}C_6 , TiC, and Ni_3Al precipitates in Nimonic263 alloy. Again, these carbides oxidize and form corresponding oxides. Thus, reactions (4, 6, 14), and from (30) to (39) will continue till the Na_2SO_4 completely exhausted into reactions under both salt mixture conditions.

Hence, hot corrosion mechanisms operative in Nimonic263 with 3SM and 3SM-A at 800 °C are fluxing, sulfidation followed by oxidation, chlorination, and high-temperature oxidation. However, it is important to emphasize that fluxing

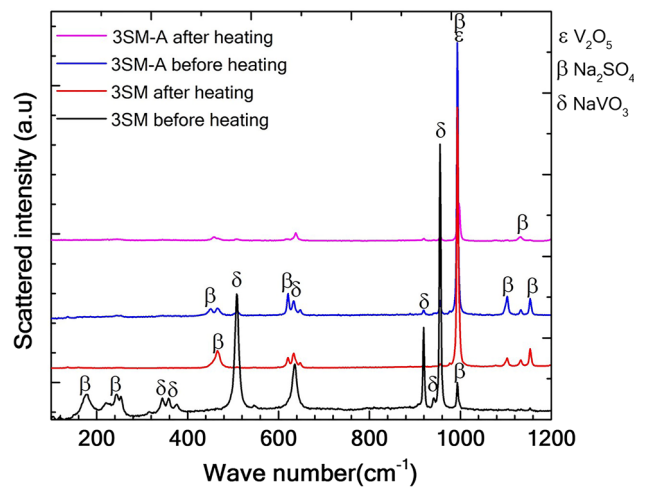


Fig. 13 Raman spectroscopy analysis of three salt mixtures (3SM and 3SM-A) annealed at 800 °C for 1 h without Nimonic263, illustrating that the constituents of 3SM-A go into a molten state much faster than 3SM

mechanism and sulfidation followed by oxidation are operative till 100 h with 3SM and 3SM-A. Moreover, the sulfidation followed by oxidation occurs with 3SM from 200 to 500 h as well as with 3SM-A during 100-200 h. Further, high-temperature oxidation takes place under the influence of 3SM-A from 300 to 500 h. Chlorination and high-temperature oxidation mechanisms are also operative in 3SM-A condition.

4.2 Why Hot Corrosion of Nimonic263 at 800 °C is More Accelerated with 3SM-A Salt Mixture than with 3SM

The difference in hot corrosion behavior of Nimonic263 coated with 3SM: 87.5 wt.% Na_2SO_4 + 5 wt.% NaCl + 7.5 wt.% NaVO_3 and 3SM-A: 74 wt.% Na_2SO_4 + 21.7 wt.% NaCl + 4.3 wt.% NaVO_3 is explained in the following section. Based on the phase diagrams of Na_2SO_4 - NaVO_3 and Na_2SO_4 -NaCl (Fig. A1 and A2) and Raman analysis for 3SM and 3SM-A at 800 °C for 1 h (Fig. 13), it is confirmed that 3SM-A salt mixture participates more actively than 3SM salt mixture and is also shown schematically in Stage I of Fig. 11. The contrasting difference between 3SM and 3SM-A stems from the difference in the weight percentages of individual salt constituents.

The amount of Na_2SO_4 of 3SM turning into molten state is lower as compared to that of 3SM-A, and consequently, Na_2SO_4 participates in hot corrosion in sequential manner (Stage III of Fig. 11 in 3SM condition), which was corroborated by the Raman analysis of 3SM (Fig. 4a) and is shown in Fig. 13. However, in contrast, with 3SM-A combination, all three constituents go into a molten state at the same time at 800 °C and participate in the hot corrosion since the eutectic point of 3SM-A is ~ 620 °C as evident from the Na_2SO_4 -NaCl phase diagram (Fig. A2). Further, with 3SM-A combination, it is more likely that SO_4^{2-} ions turn into SO_3 and oxyanions in the presence of molten NaVO_3 as shown in Stage I of Fig. 11 and same observation was also reported by Seiersten and Kofstad (Ref 49).

The compounds $\text{Na}_2\text{Cr}_2\text{O}_7$ and NaClO_3 are the volatile compounds responsible for weight loss in 3SM condition, whereas CrMoO_3 and Mo_4O_{11} are additional volatile compounds under 3SM-A condition (Fig. 3). Such contrasting

Table 4 Standard free energy formation of chlorides and oxides at 800 °C (Ref 46)

Reactions		Line equation $\Delta G^\circ_f = A + BT \log T + CT$ (in kJ/mol)	Standard free energy (ΔG°) in kJ/mol at 800 °C	
Chlorination of metals				
Cr + Cl ₂ (g)	→	CrCl ₂ (s)	-392.88 - 0.04T log T + 0.23T	- 276.2
Co + Cl ₂ (g)	→	CoCl ₂ (l)	-302.08 - 0.04T log T + 0.23T	- 185.4
2CoCl ₂ (l) + Cl ₂ (g)	→	2CoCl ₃ (g)	-141.42 + 0.15T	19.5
Ti + 2Cl ₂	→	TiCl ₄ (g)	-756.04 - 0.01T log T + 0.14T	- 638.4
Oxidation of Metals				
2Cr + 3/2O ₂	→	Cr ₂ O ₃	-1120.27 + 0.26T	- 841.3
2Co + O ₂	→	2CoO	-467.77 + 0.14T	- 317.6
3CoO + 1/2O ₂	→	Co ₃ O ₄	-183.26 + 0.15T	- 22.3
Ni + 1/2O ₂	→	NiO	-234.36 + 0.09T	- 137.8

behavior between 3SM and 3SM-A is due to the following reasons. Under 3SM-A conditions, SO₄²⁻ ions also start to attack along with VO₃⁻ and Cl⁻ ions, whereas in 3SM, these ions attack in a sequential manner, i.e., first VO₃⁻ ions and then Cl⁻ and subsequently SO₄²⁻ ions attack takes place. Consequently, sulfides are observed only up to 200 h just under the 3SM-A condition, whereas sulfides are observed up to 500 h under 3SM condition.

In 3SM condition, there is a possibility to form NaVO₃ by a combination of Na₂SO₄ and V₂O₅ as shown in Stage IV of Fig. 11 which is also consistent with thermodynamic phase stability of Na₂SO₄-V₂O₅ phase diagram by Otero et al. (Ref 50). However, in 3SM-A condition, due to the high weight percentage of NaCl, it does not allow forming protective oxides, resulting in O penetration more into the substrate and subsequently reacting with alloying elements from phases and forming corresponding volatile compounds. Thus, sulfides plus internal oxide zone of 3SM-A is very large as compared to that with 3SM (Fig. 6d). Furthermore, during 300-500 h of duration, it is anticipated that due to the thermal expansion coefficient difference between the substrate and oxides and sulfides together, spallation takes place. In addition, because of fluxing and sulfidation following oxidation, more pits will form, and subsequently, porous oxides of alloying elements will form on the top surfaces. Consequently, the metal loss will occur during 300-500 h with 3SM-A. Although EPMA mapping of 3SM-A in Fig. 8(f) shows some sulfides inside the substrate, XRD analysis (Fig. 3b) shows only oxides. It is anticipated that it is uncommon for sulfidation to take place followed by oxidation since localized equilibrium does not take place. So, oxides will easily form on the degradable Nimonic263 substrate with porous nature as shown in Fig. 6. Thus, in case 3SM-A, attack of Na₂SO₄ in parallel occurs along with NaCl (Chlorination) and NaVO₃, whereas attack of Na₂SO₄ takes place after NaCl and NaVO₃ in 3SM. Consequently, 3SM-A is more detrimental in accelerating the hot corrosion than 3SM. Owing to parallel attack with 3SM-A, alloying elements of Nimonic263 largely contribute to hot corrosion.

5. Conclusions

Isothermal hot corrosion studies at 800 °C for a duration of 500 h were carried out on Nimonic263 coated with two different 3 salt mixture combinations of 3SM: 87.5 wt.% Na₂SO₄ + 5 wt.% NaCl + 7.5 wt.% NaVO₃, and 3SM-A: 74

wt.% Na₂SO₄ + 21.7 wt.% NaCl + 4.3 wt.% NaVO₃. Based on the critical analysis of XRD patterns, BSE-SEM characterization of top and cross sections, Raman spectroscopy, cross-sectional EPMA studies, and based on the detailed discussion, the following conclusions can be drawn from the above study,

1. Pure oxidation shows weight gain up to 500 h. However, weight gain up to 25 h and then weight loss till 500 h were observed with 3SM, whereas with 3SM-A, more weight loss from 1 to 200 h and subsequently metal loss occur from 300 to 500 h. It indicates that 3SM-A salt mixture is more aggressive than 3SM.
2. Most of the corrosion products formed are with the alloying elements of Nimonic263 substrate.
3. The presence of Na₂SO₄ up to 400 h with 3SM and the formation of additional compounds NiS and AlVO₄ with 3SM-A were confirmed by Raman spectra analysis. It suggests that Ni₃Al precipitates contribute to hot corrosion. Further, Na₂SO₄ of 3SM-A disappeared from the top surface within 5 h after the exposure.
4. The alloying elements Ti, Al, and Mo participated in the reactions along with Cr as demonstrated by comprehensive EPMA analysis.
5. The higher amount of NaCl presence in 3SM-A is attributed to a more aggressive attack as compared to 3SM. Such an aggressive attack by 3SM-A resulted in forming volatile compounds and metal chlorides such as Na_{0.9}Mo₆O₁₇, CrMoO₃ and Mo₄O₁₁ and NaClO₃. These volatile compounds are responsible for more weight loss under 3SM-A condition.
6. Both fluxing and sulfidation followed by oxidation mechanisms are operative for 100 h in both 3SM and 3SM-A conditions. Sulfidation followed by oxidation mechanism is dominant for 200-500 h in 3SM and for 200 h in 3SM-A condition. During 300-500 h, high-temperature oxidation is the dominant mechanism in 3SM-A condition.
7. In addition, chlorination and high-temperature oxidation occur in 3SM-A condition.

Acknowledgments

Authors would like to thank Dr. M. Premkumar, Scientist-D, and Mr. Nikentan Vaidya, a Technical officer of DMRL, for their help in facilitating the EPMA facility and their valuable time to conduct EPMA characterization on hot corroded specimens.

References

1. M. McLean, Nickel-Base Superalloys: Current Status and Potential, *Phil. Trans. R. Soc. Lond.*, 1995, **351A**, p 419–433
2. K.L. Luthra and H.S. Spacil, Impurity Deposits in Gas Turbines from Fuels Containing Sodium and Vanadium, *J. Electrochem. Soc.*, 1982, **129**, p 649–656
3. N. Eliaz, G. Shemesh, and R.M. Latanision, Hot Corrosion in Gas Turbine Components, *Eng. Fail. Anal.*, 2002, **9**, p 31–43
4. A.U. Seybolt, Contribution to the Study of Hot Corrosion, *Trans. Met. Soc. AIME*, 1968, **242**, p 1955–1961
5. N.S. Bornstein and M.A. DeCrescente, The Role of Sodium in the Accelerated Oxidation Phenomenon Termed Sulfidation, *Metall. Mater. Trans.*, 1971, **2**, p 2875–2883
6. N.S. Bornstein and M.A. DeCrescente, The Relationship Between Compounds of Sulfur and Sulfidation, *Trans. Met. Soc. AIME*, 1969, **245**, p 1947–1952
7. J.A. Goebel, F.S. Pettit, and G.W. Goward, Mechanisms for the Hot Corrosion of Nickel-Base Alloys, *Metall. Mater. Trans.*, 1973, **4**, p 261–278
8. J.A. Goebel and F.S. Pettit, Na₂SO₄-induced Accelerated Oxidation (Hot Corrosion) of Nickel, *Metall. Mater. Trans.*, 1970, **1**, p 1943–1954
9. T.S. Sidhu, S. Prakash, and R.D. Agrawal, Hot Corrosion Behavior of HVOF-sprayed NiCrBSi Coatings on Ni- and Fe-Based Superalloys in Na₂SO₄-60% V₂O₅ Environment at 900 °C, *Acta Mater.*, 2006, **54**, p 773–784
10. R.A. Mahesh, R. Jayaganthan, and S. Prakash, Study on Hot Corrosion Behavior of Ni-5Al Coatings on Ni- and Fe-Based Superalloys in an Aggressive Environment at 900 °C, *J. Alloys Compd.*, 2008, **460**, p 220–231
11. S. Kamal, R. Jayaganthan, S. Prakash, and S. Kumar, Hot Corrosion Behavior of Detonation Gun Sprayed Cr₃C₂-NiCr Coatings on Ni and Fe-Based Superalloys in Na₂SO₄-60% V₂O₅ Environment at 900 °C, *J. Alloys Compd.*, 2008, **463**, p 358–372
12. S. Kamal, R. Jayaganthan, and S. Prakash, High-Temperature Oxidation Studies of Detonation Gun Sprayed Cr₃C₂-NiCr Coatings on Ni and Fe-Based Superalloys in Air Under Cyclic Conditions at 900 °C, *J. Alloys Compd.*, 2009, **472**, p 378–389
13. J.B. Johnson, J.R. Nicholls, R.C. Hurst, and P. Hancock, The Mechanical Properties of Surface Scales on Nickel-Base Superalloys-II. Contaminant Corrosion, *Corros. Sci.*, 1978, **18**, p 543–553
14. D.J. Wortman, R.E. Fryxell, K.L. Luthra, and P.A. Bergman, Mechanism of Low-Temperature Hot Corrosion: Burner Rig Studies, *Thin Solid Films*, 1979, **64**, p 281–288
15. K.L. Luthra, Low-Temperature Hot Corrosion of Cobalt-Based Alloys: Part I. Morphology of the Reaction Product, *Metall. Mater. Trans. A.*, 1982, **13**, p 1843–1852
16. K.L. Luthra, Low-Temperature Hot Corrosion of Cobalt-Based Alloys: Part II. Reaction Mechanism, *Metall. Mater. Trans. A.*, 1982, **13**, p 1853–1864
17. S. Kameswari, The Role of NaCl in the Hot-Corrosion Behavior of the Nimonic Alloy 90, *Oxid. Met.*, 1986, **26**, p 33–44
18. J.R. Nicholls and D.J. Stephenson, A Life Prediction Model for Coatings Based on the Statistical Analysis of Hot Salt Corrosion Performance, *Corros. Sci.*, 1992, **33**, p 1313–1325
19. C.A.C. Sequeira and M.G. Hocking, Hot Corrosion of Nimonic 105 in Sodium Sulfate-Sodium Chloride Melts, *Corrosion*, 1981, **37**, p 392–407
20. R. Sivakumar, P.K. Sagar, and M.L. Bhatia, On the Electrochemical Nature of the Hot-Corrosion Attack in Ni-Cr Alloys, *Oxid. Met.*, 1985, **24**, p 315–330
21. I. Gurrappa, Hot Corrosion Behavior of CM 247 LC Alloy in Na₂SO₄ and NaCl Environments, *Oxid. Met.*, 1999, **51**, p 353–382
22. C.L. Zeng and T. Zhang, Electrochemical Impedance Study of Corrosion of B-1900 Alloy in the Presence of a Solid Na₂SO₄ and a Liquid 25 wt.% NaCl-75 wt.% Na₂SO₄ Film at 800 °C in air, *Electrochim. Acta.*, 2004, **49**, p 1429–1433
23. Meiheng Li, Xiaofeng Sun, Hu Wangyu, Hengrong Guan, and Shuguang Chen, Hot Corrosion of a Single Crystal Ni-Base Superalloy by Na-Salts at 900 °C, *Oxid. Met.*, 2006, **65**, p 137–150
24. G.M. Liu, F. Yub, J.H. Tian, and J.H. Ma, Influence of Pre-oxidation on the Hot Corrosion of M38G Superalloy in the Mixture of Na₂SO₄-NaCl Melts, *Mater. Sci. Eng. A*, 2008, **496**, p 40–44
25. T.S. Sidhu, A. Malik, S. Prakash, and R.D. Agrawal, Cyclic Oxidation Behavior of Ni- and Fe-Based Superalloys in the Air and Na₂SO₄-25%NaCl Molten Salt Environment at 800 °C, *Int. J. Phys. Sci.*, 2006, **1**, p 27–33
26. K. Zhang, M.M. Liu, S.L. Liu, C. Sun, and F.H. Wang, Hot Corrosion Behavior of a Cobalt-Base Super-Alloy K40S with and without NiCrAlYSi Coating, *Corros. Sci.*, 2011, **53**, p 1990–1998
27. Lei Zheng, Zhang Maicanga, and Dong Jianxin, Hot Corrosion Behavior of Powder Metallurgy Rene 95 Nickel-Based Superalloy in Molten NaCl-Na₂SO₄ Salts, *Mater. Des.*, 2011, **32**, p 1981–1989
28. G.S. Mahobia, Neeta Paulose and Vakil Singh, Hot Corrosion Behavior of Superalloy IN718 at 550 and 650 °C, *J. Mater. Eng. Perform.*, 2013, **22**, p 2418–2435
29. V. Mannava, A.S. Rao, N. Paulose, M. Kamaraj, and R.S. Kottada, Hot Corrosion Studies on Ni-Base Superalloy at 650 °C Under Marine-like Environment Conditions Using Three Salt Mixture (Na₂SO₄+NaCl+NaVO₃), *Corros. Sci.*, 2016, **105**, p 109–119
30. M.S. Doolabi, B. Ghasemi, S.K. Sadmezhaad, A. Habibollahzadeh, and K. Jafarzadeh, Hot Corrosion Behavior and Near-Surface Microstructure of a Low-Temperature High-Activity Cr-Aluminide Coating on Inconel 738LC Exposed to Na₂SO₄, Na₂SO₄ + V₂O₅, and Na₂SO₄ + V₂O₅ + NaCl at 900 °C, *Corros. Sci.*, 2017, **128**, p 42–53
31. Dhananjay Pradhan, G.S. Mahobia, K. Chattopadhyay, and V. Singh, Effect of Surface Roughness on Corrosion Behavior of the Superalloy IN718 in the Simulated Marine Environment, *J. Alloys Compd.*, 2018, **740**, p 250–263
32. D. Pradhan, G.S. Mahobia, K. Chattopadhyay, and V. Singh, Severe Hot Corrosion of the Superalloy IN718 in Mixed Salts of Na₂SO₄ and V₂O₅ at 750 °C, *J. Mater. Eng. Perform.*, 2018, **27**, p 4235–4243
33. F. Saegusa and D.A. Shores, The Corrosion Resistance of Superalloys in Temperature Range of 800–1300 °F, *J. Mater. Energy Syst.*, 1982, **4**, p 16–27
34. A. Manonukul and D. Knowles, A Physically-Based Model for Creep in Nickel-Base Superalloy C263 both above and below the Gamma Solvus, *Acta Mater.*, 2002, **50**, p 2917–2931
35. V. Mannava, A.V. Swaminathan, M. Kamaraj, and R.S. Kottada, An Innovative Spraying Setup to Obtain Uniform Salt(s) Mixture Deposition to Investigate Hot Corrosion, *Rev. Sci. Instrum.*, 2016, **87**, p 25107
36. B.D. Hosterman, Raman Spectroscopic Study of Solid Solution Spinel Oxides, Ph.D. Thesis, University of Nevada, Las Vegas, 2016
37. D. Zákutná, A. Repko, I. Matulková, D. Nižňanský, A. Ardu, C. Cannas, A. Mantlíková, and J. Vejpravová, Hydrothermal Synthesis, Characterization, and Magnetic Properties of Cobalt Chromite Nanoparticles, *J. Nanopart. Res.*, 2014, **16**(2251), p 1–14
38. D.W. Bishop, P.S. Thomas, and A.S. Ray, Raman Spectra of Nickel (II) Sulfide, *Mater. Res. Bull.*, 1998, **33**, p 1303–1306
39. B.L. Hurley, S. Qiu, and R.G. Buchheit, Raman Spectroscopy Characterization of Aqueous Vanadate Species Interaction with Aluminum Alloy 2024-T3 Surfaces, *J. Electrochem. Soc.*, 2011, **158**, p C125–C131
40. Laura E. Briand, Jih-Mirn Jehng, Laura Cornaglia, Andrew M. Hirt, and Israel E. Wachs, Quantitative Determination of the Number of Surface Active Sites and the Turnover Frequencies for Methanol Oxidation Over Bulk Metal Vanadates, *Catal. Today*, 2003, **78**, p 257–268
41. V.G. Hadjiev, M.N. Iliev, and I.V. Vergilov, The Raman Spectra of Co₃O₄, *J. Phys. C: Solid State Phys.*, 1988, **21**, p L199–L201
42. B.-K. Choi and D.J. Lockwood, Raman Spectrum of Na₂SO₄ (Phases I, and II), *Solid State Commun.*, 1990, **76**, p 863–866
43. B.-K. Choi and D.J. Lockwood, Raman Spectrum of Na₂SO₄ (Phase V), *Solid State Commun.*, 1989, **72**, p 133–137
44. K.S. Ghosh and S. Raghavan, Fusion Point Diagram of Na₂SO₄-NaVO₃-NaCl System, *Trans. Indian Inst. Metals.*, 1995, **48**, p 401–408
45. P.S. Sidky and M.G. Hocking, The Hot Corrosion of Ni-Based Ternary Alloys and Superalloys for Application in Gas Turbines Employing Residual Fuels, *Corros. Sci.*, 1987, **27**, p 499–530
46. O. Kubaschewski and C.B. Alcock, *Metallurgical Thermo-Chemistry*, revised, 5th ed., Pergamon Press Publisher, New York, 1983
47. C.C. Tsaur, J.C. Rock, C.J. Wang, and Y.H. Su, The Hot Corrosion of 310 Stainless Steel with Pre-coated NaCl/Na₂SO₄ Mixtures at 750 °C, *Mater. Chem. Phys.*, 2005, **89**, p 445–453
48. R.A. Rapp, Hot Corrosion of Materials: a Fluxing Mechanism?, *Corros. Sci.*, 2002, **44**, p 209–221
49. M. Seiersten and P. Kofstad, The Effect of SO₃ on Vanadate-Induced Hot Corrosion, *High Temp. Technol.*, 1984, **5**, p 115–122
50. E. Otero, A. Pardo, J. Hernaez, and F.J. Perez, The Hot Corrosion of in-657 Superalloy in Na₂SO₄-V₂O₅ Melt Eutectic, *Corros. Sci.*, 1991, **32**, p 677–683